Deformation Mechanisms and Plastic Resistance in Single-Crystal-Textured High-Density Polyethylene

Z. Bartczak,† A. S. Argon,*,‡ and R. E. Cohen*,§

Departments of Chemical and Mechanical Engineering, Massachusetts Institute of Technology, Cambridge, Massachusetts 02139

Received January 13, 1992; Revised Manuscript Received May 7, 1992

ABSTRACT: Highly textured high-density polyethylene (HDPE) prepared by plane strain compression in a channel die was used as a macroscopic approximation to a single crystalline material to study the plastic deformation mechanisms. Samples cut out of the textured rectangular bars were subjected to tensile, compressive, and simple shear deformation in different crystallographic orientations, specifically chosen to probe the deformation resistances of specific crystallographic mechanisms of deformation. The degree of dominance of specific mechanisms in certain ranges of crystal orientation was ascertained by WAXS and SAXS measurements together with measurements of incremental shape changes of deformed samples. Through these studies it was determined that in deformation orientations requiring chain slip the most dominant mechanism was (100)[001] chain slip, with (010)[001] chain slip being a frequent alternative. Only scant evidence was found for the activity of (110)[001] chain slip. In deformation orientations requiring transverse slip evidence was found for the presence of (100)[010] transverse slip. In such orientations, however, very clear evidence was found also for deformation twinning on (110) planes. Martensitic transformations were not detected in any of the experiments. In compression experiments with the compression axis making a small angle with the chain axis and in tension experiments with the tensile axis making a large angle with the chain axis, chain slip often manifested itself in the formation of prominent kink bands. Shear resistances of the prominent slip systems and twinning systems together with their normal stress dependences at room temperature are reported together with considerably detailed descriptions of the observed kinematical modes of the specific deformation mechanisms.

1. Introduction

A large amount of attention has been given to theoretical and experimental aspects of deformation mechanisms in semicrystalline polymers.[1-4] The plastic deformation of such polymers is a complex process; many competing phenomena are likely to occur simultaneously when such a polymer is plastically deformed. In semicrystalline polymers crystalline lamellae, separated by amorphous layers and connected by tie molecules, are arranged spatially to form spherulites or other morphological forms. Thus, the plastic deformation of semicrystalline polymers has to be described at different levels: individual lamellar crystals, stacks of lamellae, spherulites, etc. It is particularly interesting to study the deformation behavior of the crystalline component. This can be done either in single crystals on the microscopic level or in macroscopic samples if an oriented polymer with well-defined quasi-single-crystal texture is available for study. In the latter material, the spherulitic superstructure has been replaced by an aligned molecular structure through an orientation process in which reconstituted lamellae are arranged parallel to each other throughout the sample and where the chain axes are aligned along the orientation direction associated with the large-strain deformation process.

Many of the investigations of the mechanisms of deformation in oriented semicrystalline polymers have been concerned with high-density polyethylene (HDPE). Similar to other crystalline polymers, HDPE can deform plastically by crystallographic slip, twinning, or stress-induced martensitic transformations as well as by deformation of the amorphous phase. Fine chain slip (i.e., the translation of individual molecules past each other along the molecular axis) occurs homogeneously within crystalline lamella, rotating both the chain axis and lamella surface by shear.[7] This mechanism has been found to dominate the deformation of oriented HDPE.[5-10] Theoretical considerations, supported by experimental observation of the deformation of single crystals,[1] predict the possibility of any (*hk*0)[001] chain slip (i.e., slip on any (*hk*0) plane in the molecular axis direction [001]). Based on the fact that deformation of all crystalline materials tends to occur along a close-packed plane in the structure[1] and relying on some energetic considerations,[11] the (100), (010), and (110) planes are anticipated to be the preferred planes for chain slip in polyethylene crystals. Of these the (100)[001] slip is expected to have the lowest resistance to deformation. Experimental studies have shown that the two most important chain slip modes are (100)[001] and (010)[001] fine chain slip.[1,2] The third slip system on the (110) plane has not been detected experimentally in oriented HDPE. Coarse chain slip and fibrillar slip (slip in the chain direction but localized within the lamellar crystal to a few planes or between preexisting fibrillar stacks of lamellae) have also been proposed as mechanisms of deformation in HDPE.[12]

In addition to these processes which all give rise to macroscopic shear parallel to the molecular direction, there are three mechanisms giving rise to shear normal to the molecular axis. Oriented HDPE, when compressed normal to the chain direction, undergoes (100)[010] transverse slip (slip on the (100) plane in the [010] direction, normal to the molecular axis).[13] Other possible transverse slip systems in polyethylene have been considered by Frank et al.[14] The closest packed direction is [010] so this may be expected to be the direction of easiest transverse slip; [100] is the next longest. Since the (010)[100] system is orthogonal to (100)[010], the resolved shear stress on both systems is the same, so that (100)[010] will always be preferred, if it indeed has a lower resistance, as expected. Slip on the third possible system (110)[1$\bar{1}$0] is more difficult because it involves a large Burgers vector.

† Permanent address: Centre of Molecular and Macromolecular Studies, Polish Academy of Sciences, 90-362 Lodz, Poland.
‡ Department of Mechanical Engineering.
§ Department of Chemical Engineering.

0024-9297/92/2225-5036$03.00/0

Moreover, it is always in competition with the 110 twinning modes and thus may not be observed. Twinning on the (110) planes has been found to occur during compression of oriented HDPE[13] as well as in polyethylene single crystals.[15] In drawn bulk HDPE, evidence of {310} twinning was also found.[16] A stress-induced martensitic transformation was reported for both single crystals and oriented HDPE.[13,15] Besides the deformation in the crystalline component, two modes of deformation within the amorphous layers have been proposed: interlamellar sliding and lamellar separation.[9,10]

The above-mentioned studies have revealed the principal deformation mechanisms of semicrystalline HDPE. However, relatively less attention has been placed on obtaining quantitative information about particular deformation mechanisms, which is necessary to predict the deformation behavior of the polymer in a given stress state. In some previous studies, the effect of applying tensile or compressive stress at different angles to the molecular alignment direction has been used in order to find the yield criterion and the plastic resistances for the deformation of polymer crystals.[5-7,10,13,17,18] Various yield criteria such as the Schmid law,[7,13,18] the Coulomb criterion,[5,6] the Hill–von Mises criterion,[17] and a fiber composite model[17] were applied to fit experimental data. The Coulomb yield criterion, in contrast to the Schmid law or the Hill–von Mises criterion, includes a dependence of the shear yield stress on normal stress or pressure. [For initiation of plasticity a number of critical stress criteria have been introduced in the past. Breifly, these can be stated as follows. (a) Schmid law: Plastic shear is initiated in a crystalline material when the resolved shear stress on a slip plane in a slip direction reaches a critical value. (b) Hill–von Mises criterion: Plastic deformation in a polycrystalline solid is initiated when the second invariant of the local stress reaches a critical value called the plastic resistance. (c) Coulomb criterion: The critical resolved shear stress (Schmid law) or the plastic shear resistance (Hill–von Mises criterion) may increase linearly with the normal compression stress for the shear plane or with the local prevailing pressure.]

The aim of the present work was to determine the plastic resistances for the three most important mechanisms acting in HDPE, i.e., the (100)[001] and (010)[001] chain slips and (100)[010] transverse slip, and to explore ranges of crystal orientation in which a single one of these mechanisms dominates the observed deformation behavior. An attempt was also made to detect the (110)[001] chain slip, which according to theoretical predictions should also be an active mechanism in the deformation of polyethylene crystals.

Plastic flow of HDPE in a channel die leads to a highly oriented material of macroscopic dimensions with a quasi-single-crystal texture[20] which provides an ideal starting point for the present study. The yield behavior of a particular slip mode may then be studied by deforming specially prepared tensile or compression specimens of specific orientations cut from the oriented material in such a way as to activate a single deformation mechanism and explore its properties. Thus, in order to test the applicability of one or the other of the yield criteria and to obtain accurate information on given slip resistances, we investigated the deformation behavior of textured HDPE using specimens covering a wide range of angles between the initial orientation direction and the load direction as well as in various deformation conditions, i.e., uniaxial tension, uniaxial compression, and simple shear. In what follows we report these new findings.

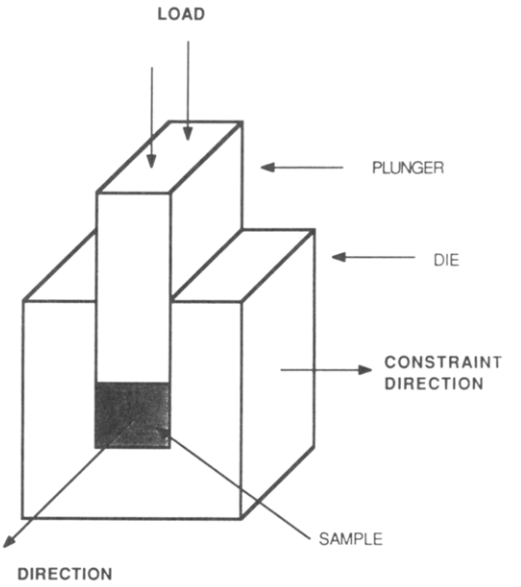

Figure 1. Channel-die device for quasi-single-crystal sample preparation by plane strain compression.

2. Experimental Section

2.1. Materials and Sample Preparation. The material used in this study was high-density polyethylene (HDPE), Petrothene LS 606-00, supplied by Quantum, USI Division, Cincinnati, OH. Its molecular weight was $M_w = 55\,000$ with a polydispersity ratio $M_w/M_n = 4.8$, a melt flow index of 9–11 g/10 min (ASTM D-1238), and a density of 0.941–0.980 g/cm^3.

The polymer pellets were compression molded at 180 °C and 100 atm pressure to form a plate of ca. 20-mm thickness, from which a 72 mm × 75 mm × 10 mm thick core was machined. This plate was oriented by plane strain compression in a channel die[19,20] (see Figure 1), in which the surfaces were lubricated using Dow Corning 44 high-temperature grease. The compression was performed at 80 °C and at a deformation rate of 2.5×10^{-3} s^{-1} to a compression ratio of $\lambda = 6$ (reduction from 72 to 12 mm). The sample was then slowly cooled to room temperature without removing it from the channel die. The oriented bar specimens (12 × 10 × 75 mm) were subsequently annealed for 6 h at 117 °C in the constrained state. The HDPE prepared according to the above procedure shows a quasi-single-crystal texture, with chain axis c being well oriented along the flow direction (FD), the a-axis along the loading direction (LD), and the b-axis along the constraint direction (CD).[20]

2.2. Slip Resistance Measurements. A. Specimen geometry: The deformation behavior of the quasi-single-crystal-textured HDPE was studied in three deformation modes: uniaxial tension, uniaxial compression, and simple shear to probe individual slip systems selectively. The intention was to prepare the specimens such that only one of the various possible deformation mechanisms could be activated, the others being rendered inactive because of constraints imposed by the specimen orientation and geometry. The orientations appropriate to study particular slip systems were selected on the basis of analysis of the expected dependencies of resolved shear stress for these systems on the direction of the load, presented in the Appendix. Four crystallographic slips were targeted for study in this way: (100)[001] chain slip, (010)[001] chain slip, (110)[001] chain slip, and (100)[010] transverse slip.

The oar-shaped tensile specimens had a gauge length of 2.38 mm, a width of ~1.5 mm, and a thickness of ~0.7 mm. In order to activate any particular slip mode, specimens were machined from the bar of textured HDPE as shown in Figure 2. The expected plane of slip in each instance was perpendicular to the specimen surface and formed an acute angle with the tensile axis. The angle θ, between the tensile axis and the direction of expected slip (c-axis for chain slips and b-axis for transverse slip) was varied from 0 to 90° in order to test the validity of the Coulomb yield criterion, which appeared to be the most promising.

The specimens for compression tests had a rectangular shape with a height of ~5 mm, a width of ~3 mm, and a thickness

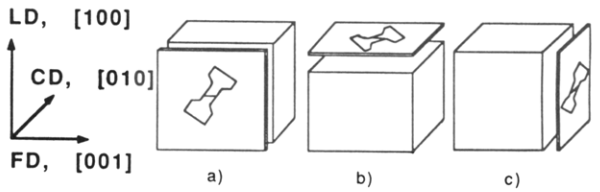

Figure 2. Method of cutting the tensile specimens for study of various deformation mechanisms: (a) (100)[001] chain slip; (b) (010)[001] chain slip; (c) (100)[010] transverse slip.

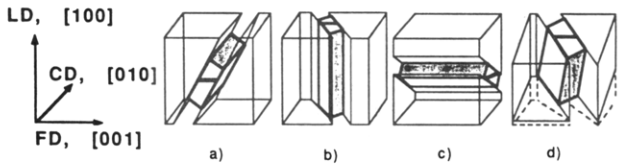

Figure 3. Method of cutting the compression specimens for study of various deformation mechanisms: (a) (100)[001] chain slip; (b) (010)[001] chain slip; (c) (100)[010] transverse slip; (d) (110)[001] chain slip.

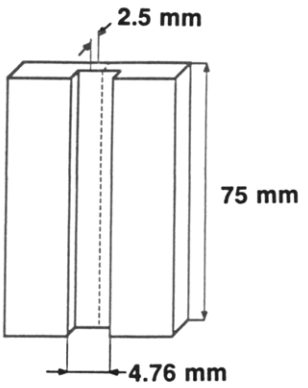

Figure 4. Geometry of the specimen for the simple shear experiment.

greater than 10 mm. Figure 3 illustrates the method of cutting the specimens from the textured HDPE sample. Similar to the tensile specimens the angle θ between the compression axis and the slip direction was varied from 0 to 90°. The thickness of the compression specimens was large compared to their width in order to constrain any other deformation, especially slip on oblique planes giving out-of-plane deformation.

The simple shear experiments were performed with specimens in which the plane of shear was (100), (010), or (110) and the direction of shear was along the c-axis. In this way it was possible to study the (100)[001], (010)[001], and (110)[001] chain slips, respectively. The geometry and dimensions of shear specimens are shown in Figure 4. The specimen dimensions were selected according to the criteria discussed by G'Sell et al.[21]

For simplicity in further discussion, the specimens with geometry promoting a particular slip mode $(hkl)[h_1k_1l_1]$ will be called $(hkl)[h_1k_1l_1]$ specimens (i.e., (100)[001] specimens and (010)[001] specimens for the study of chain slip modes and (100)-[010] specimens to study transverse slip).

B. Preparation of specimens: All specimens for mechanical testing were prepared using similar procedures. First they were machined from the bar of textured HDPE with appropriate orientation and shape. During this operation the material was mounted on a support plate using double-coated adhesive tape and additionally reinforced laterally with an epoxy resin. Such mounting eliminated any need for gripping of the sample, which could induce some unwanted transformation, e.g., martensitic transformation or mechanical twinning of the material due to compressive forces. During machining, the sample and the cutting tool were continuously cooled with water in order to avoid any morphological changes in the specimen induced by heat or large cutting forces. After machining the surfaces, specimens were rough ground with wet, 600-mesh silicon carbide abrasive paper and then carefully polished with 1-, 0.3-, and finally 0.05-μm aluminum oxide powder suspended in water. In tensile specimens all edges were carefully polished, to suppress unwanted premature fracture.

C. Testing: The mechanical tests were carried out using a Model 4201 Instron tensile testing machine. The initial deformation rate for all types of tests was 4.2×10^{-4} s^{-1}. Both tensile and compression tests were performed using standard Instron equipment (pneumatic action tensile grips, compression plates) whereas for simple shear experiments the Instron machine was equipped with a specially constructed shearing device.[21] The specimens for compression tests were lubricated on the faces contacting the compression plates of the testing machine to minimize the friction. The lubricant used was Dow Corning 44 grease.

From experimentally determined nominal stress–nominal strain curves the yield stress was calculated. Often the yield point has been defined by other investigators as a stress at maximum observed load on the load–displacement curve. However, such a maximum was not always observed in our load–displacement curves, especially for specimens tested in compression, where load frequently increases continuously with increasing compression. Therefore, an alternative definition of yield stress was used which was taken as the stress at the intersection of the measured stress–strain curve and a straight line parallel to the initial slope of the curve and offset by 4% nominal strain.[3] When the stress–strain curve of a particular specimen showed a clear stress maximum, the offset yield stress and related strain were usually close to but slightly lower than the maximum stress and strain related to the load maximum. In very few cases (compression specimens for (100)[001] chain slip, with small θ angle) the stress–strain curve had a distinct maximum (due to the development of kinking) at strains lower than that corresponding to the offset yield stress; in such cases the yield stress was taken directly from the maximum of the stress–strain curve.

2.3. X-ray Measurements. The overall orientations of crystallographic planes of the samples were determined by means of an automated computer-controlled Rigaku WAXS system consisting of a pole figure device associated with a wide-angle goniometer coupled to a rotating-anode X-ray generator (Cu Kα radiation) operating at 50 kV and 60 mA.

The small-angle X-ray scattering measurements (SAXS) were performed using another computer-controlled system consisting of a Nicolet two-dimensional position-sensitive detector and a second Rigaku rotating-anode X-ray generator (Cu Kα radiation, 40 kV and 30 mA). The primary beam was collimated by a two-mirror system so that the primary X-ray beam could be effectively focused onto a beam stop with a fine size without losing much intensity. The specimen-to-detector distance of the SAXS system was 2.3 m. The scattered X-ray path between specimen and detector was filled with He gas to minimize attenuation and background scattering.

Changes of lamellar orientation were studied by SAXS on specimens deformed directly in the SAXS camera using small compression clamps or tension jigs, so that the specimen remained under load during the measurement; unloaded specimens from mechanical tests on the Instron were also examined. The WAXS measurements using the pole figure attachment need large samples (at least 1 cm × 1 cm), so it was necessary to take several specimens, deformed previously in the Instron machine to the same strain, and glue them together in the unloaded state. These WAXS pole figure measurements were performed about 1 h after deformation and load release.

2.4. Other Techniques. A. Density measurements: Densities of the samples were determined by means of a 1-m-long gradient column filled with a mixture of ethyl alcohol and water. The temperature of the column was maintained at 23 °C.

B. Differential scanning calorimetry: A Perkin-Elmer DSC-4 apparatus was used to study the melting of the oriented specimens. The heating rate was 10 °C/min. For calculation of the overall crystallinity from DSC data the heat of fusion of 100% crystalline linear polyethylene was taken as $\Delta H_f = 293$ J/g.[22]

3. Results and Discussion

3.1. Initial Structure of Oriented HDPE. The texture of the HDPE oriented by plane strain compression

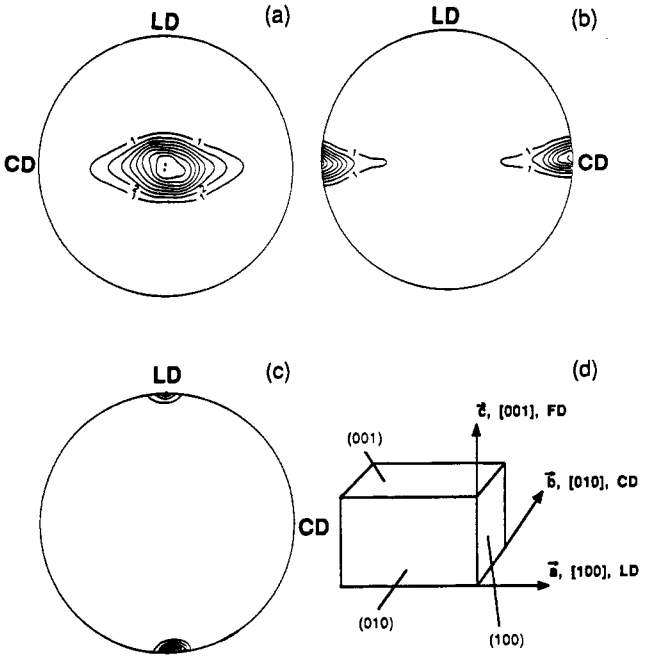

Figure 5. Pole figures of HDPE oriented by channel-die compression: (a) (002) plane; (b) (020) plane; (c) (200) plane. FD = flow direction, CD = constraint direction, and LD = load direction as shown in d.

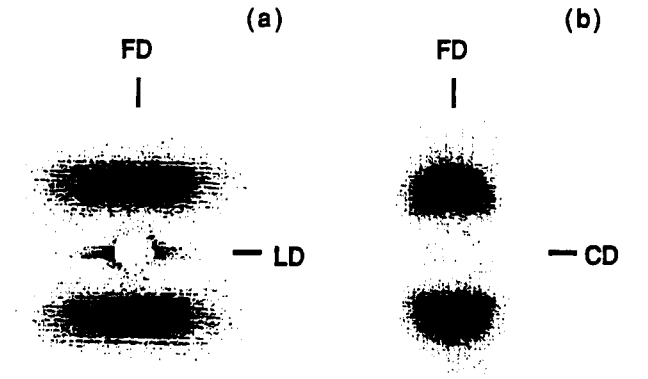

Figure 6. SAXS pattern of HDPE oriented by channel-die compression: (a) incident beam parallel to constraint direction; (b) incident beam parallel to loading direction. FD = flow direction, LD = loading direction, CD = constraint direction, all in the channel-die coordinate system.

was previously investigated in some detail by Song et al.[20] It was found that HDPE oriented in this way exhibits a quasi-single-crystal texture with the *c*-axis of crystallites oriented along the flow direction in the die, the *a*-axis along the loading direction, and the *b*-axis along the constraint direction as outlined in Figure 5, showing the pole figures of the crystallographic directions (Figure 5a–c) and as summarized in Figure 5d. As revealed by small-angle X-ray scattering (SAXS) and transmission electron microscopy (TEM), the lamellae are long in both the *a* and *b* directions (several hundred nanometers), and when viewed from the loading direction, they are arranged almost perfectly perpendicular to the flow direction. Observed from the constraint direction, however, the lamellae are either perpendicular to or tilted to the flow direction. The analysis of SAXS patterns (as well as orientation of crystallites obtained from wide-angle diffraction data) showed that even in those lamellae tilted with respect to the flow direction the chains were still aligned along the flow direction. The meridional broadening of the SAXS pattern of Figure 6a observed for samples oriented with the constraint direction parallel to incident X-ray beam suggests that there is a relatively broad distribution of orientations of long lamellae in the plane perpendicular to the constraint direction, while the crystallographic *c*-axes in every lamella remain nearly parallel to the flow direction.[20]

The present observations suggest that the description of lamellar structure[20] outlined above should be very slightly revised. TEM observations[23] of channel-die oriented HDPE samples which were not annealed after orientation (samples studied in ref 20 were annealed) showed that the lamellae observed from the constraint direction are considerably shorter than those observed in the annealed material and that the unannealed lamellae are arranged in relatively long rows, resembling the previously observed long lamellae. Such rows of adjacent short lamellae are oriented generally perpendicular to the flow direction, although the distribution of orientation is relatively broad similar to the distribution of lamellar orientations reported in ref 20. Annealing cannot cause a significant increase of lateral sizes of lamellae because the polymer is already highly crystalline (70–75%), and the lateral growth of the lamellae during the annealing procedure is limited by the presence of adjacent lamellae in the row. Thus, the final lateral sizes of lamellae are evidently not much larger than before annealing. However, as a result of annealing the noncrystalline regions between laterally adjacent lamellae narrow markedly, making them difficult to detect in the annealed sample. As a result the rows of closely packed, although still separated, lamellae may be interpreted in the TEM image as a single, long lamella. Taking everything above into consideration, the meridional broadening of SAXS patterns presented in Figure 6a should be interpreted as a result of the superposition of two factors: spatial orientation, discussed in ref 20, and the effect of the small lateral size of the lamellae, which is another common interpretation of such SAXS patterns.

Another feature of 2D SAXS patterns of HDPE oriented by plane strain compression is the equatorial streak which can be observed when the sample is oriented with its constraint direction parallel to the incident beam as in Figure 6a; equatorial scattering is not observed when the sample is oriented with the loading direction parallel to the incident beam, as is clear from Figure 6b. Such equatorial scattering in a SAXS pattern is often interpreted as a result of the presence of microvoids in the material. In order to give the observed scattering shown in Figure 6a, the microvoids must be located in planes perpendicular to the loading direction, i.e., in the (100) planes, and have a shape which is elongated in the flow direction.

To find out if voids do indeed exist in the channel-die-compressed HDPE structure, density measurements and heat of melting (DSC) measurements were performed on oriented as well as unoriented HDPE. In the density determination the position of the specimen in the gradient column was measured and the density was calculated as a function of time after immersion in the column. In addition, density was estimated from the heat of melting obtained from DSC measurements (assuming $\Delta H_f = 293$ J/g[22] and taking for the densities of crystalline and amorphous regions 1.00 and 0.855 g/cm^3, respectively). The results are presented in Table I. The density estimated from the DSC melting data is very close to that measured in the gradient column. In the case of the unoriented sample, which should be free of voids, the measured densities do not vary with time of immersion, whereas the apparent density of oriented specimens increases slightly with immersion time. This could suggest that cavities are gradually filled with the gradient column fluid. The increase in the density, is rather small, presumably because only a fraction of the cavities are connected with the specimen surface and can be filled by

Table I
Densities of Unoriented and Highly Oriented HDPE Samples Measured in a Density Column or Estimated by Means of DSC (g/cm³)

	density column (density at specified time)			
	15 min	3 h	24 h	DSC
unoriented	0.9555	0.9555	0.9555	0.9562
oriented[a]	0.9600	0.9628	0.9631	0.9629
oriented[b]	0.9658	0.9662	0.9662	0.9664

[a] Compression ratio of 6.0. [b] Compression ratio of 6.2.

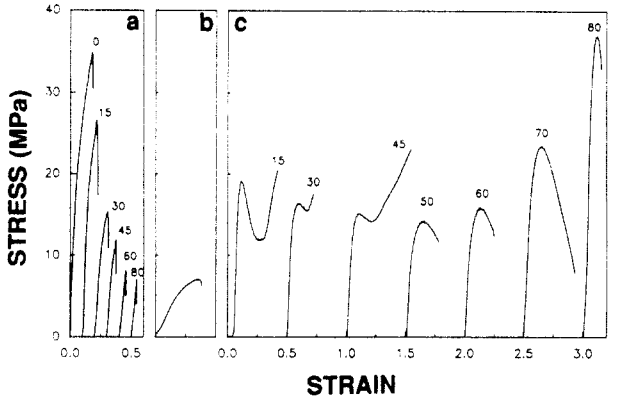

Figure 7. Typical stress–strain curves for (100)[001] specimens tested in (a) tension, (b) shear, and (c) compression. Values of θ_0 are shown near the stress–strain curves, which are displaced along the strain axis for clarity of presentation.

liquid. Additionally, if these cavities cause the scattering of the X-ray, they must be very small in size; moreover, their total volume fraction is also likely to be very small; thus, their presence does not change the specimen densities very much.

As mentioned before, the SAXS patterns suggest that the microvoids are located mainly in the plane perpendicular to the load direction and are oriented with their longer dimension along the flow direction. This is consistent with the previously discussed small lateral sizes of lamellae in the loading direction; the microvoids, most likely have been formed during the orientation of lamellae, when their fragmentation occurs. The lateral size of lamellae viewed from the loading direction is much smaller than that viewed from the constraint direction. This suggests a more intense fragmentation in the (100) plane than in the (010) plane. Thus, most of the microvoids resulting from orientation are oriented in the (100) plane, which is perpendicular to the loading direction in the final oriented material.

3.2. Deformation by (100)[001] Chain Slip. Figure 7 shows typical stress–strain curves for (100)[001] specimens tested in tension, compression, and shear experiments. As discussed in section 2.2, the orientation and size of these specimens were carefully selected in order to maximize the possibility of plastic deformation by (100)-[001] chain slip, while minimizing the possibility of activating competing deformation mechanisms in the course of the deformation test. In tensile experiments, depending on the angle θ_0 between the initial direction of the chain axis and the direction of tension, two different modes of deformation can be distinguished (see Figure 7a). Specimens with $\theta_0 \leq 20°$ broke at the yield point or very shortly after yielding, whereas specimens with $\theta_0 > 20°$ exhibited brittle behavior, fracturing before yield. The fracture was frequently initiated on the curved edge of the oar-shaped specimen beyond the gauge area where stress concentrations exist, but it always spread along the (100) crystallographic plane (or very close to this plane)

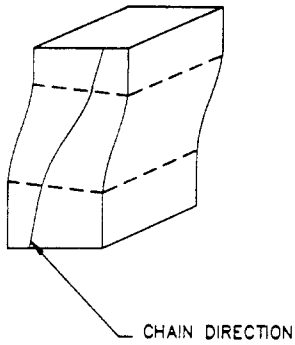

Figure 8. Geometry of the kink band formed in (100)[001] compression specimens with small θ_0 angles typical of all kinking type response.

independent of the initial specimen orientation (θ_0), suggesting the presence of some structural weakening in these planes, most likely the microvoids referred to above.

The (100)[001] samples tested in simple shear underwent yielding but fractured along the (100) plane shortly after that. However, the specimens tested in uniaxial compression showed more extensive plastic behavior, as is shown in Figure 7c, deforming up to a strain of 50% before any fracture occurred. Direct observation of the specimens during their deformation revealed that they deformed by slip in the (100) plane along the [001] direction. If the specimen fractured, the fracture surface was similar to that in the tensile specimens, i.e., parallel to the (100) plane, except for specimens with $\theta_0 > 70°$, in which the fracture surface formed an acute angle with the (010) plane, suggesting that for these specimens of large θ_0 not only was the operating deformation mechanism shear in the (100) plane but also some other mechanism was evidently involved. Measurements of the changing dimensions of compressed specimens showed that for strains as high as 40–50% the change of the specimen thickness (i.e., its longest dimension along the [010] direction; see Figure 3) was not larger than about 1.5%, whereas the relative increase in the width was close to the reduction of the specimen height. This result supports the observation that the active deformation mechanism during compression is mainly in the form of shear (slip) in the (100) plane.

In (100)[001] samples with $\theta_0 \leq 20°$ formation of macrokink bands lying in the (010) plane was observed; the geometry is shown schematically in Figure 8. Upon formation, the kink band spread over the specimen with increased compression under decreasing stress. Formation of the kink band caused a significant reorientation of chain axes in the middle of the specimen (inside the kind band) toward larger θ angles, i.e., away from the compression direction, as might be expected. As revealed by X-ray measurements this angle increased still further when the kink band had spread over the entire sample, suggesting that the deformation occurs by shear on the (100) plane inside the already formed kink band, all under decreasing nominal stress as the Schmid factor on the active system increases with rotation of the active planes away from the compression direction. We also note this effect in the distinctly different form of the stress–strain curves for orientations below $\theta_0 = 20°$. For specimens with $\theta_0 \leq 20°$ the maximum on the stress–strain curve is very distinct and appears at strains less than the strain corresponding to the 4% offset yield point. When θ_0 is larger than 20°, the maximum is less distinct and is located at strains slightly higher than the 4% offset. While kinking response was typical of all other compression samples with small θ_0 angles, not all resulted in the formation of macrokink bands.

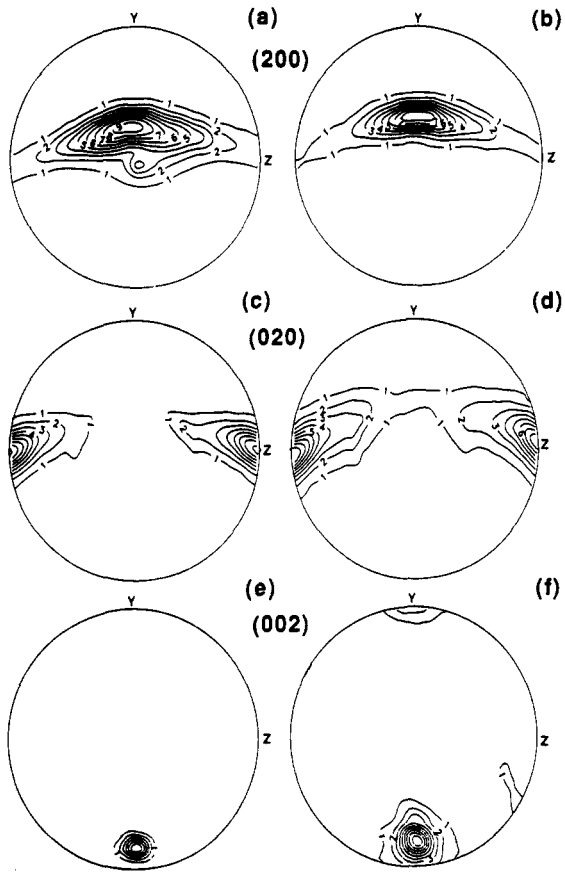

Figure 9. Pole figures of the (100)[001] compression specimen with $\theta_0 = 15°$ before deformation (a, c, e) and at 20% strain (b, d, f): (a, b) (200) plane; (c, d) (020) plane; (e, f) (002) plane. y = compression loading direction; z = plane strain constraint direction. See the inset in Figure 12 for definition of these directions.

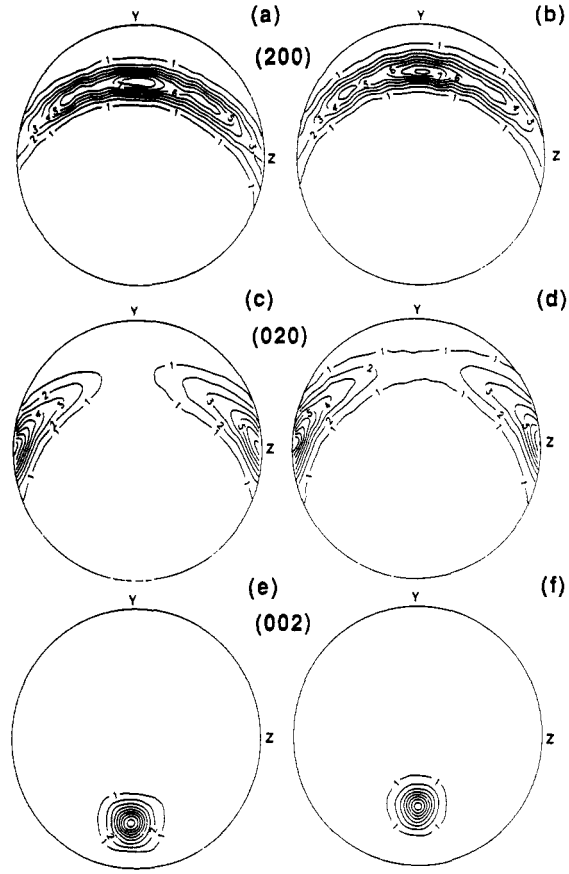

Figure 10. Pole figures of the (100)[001] compression specimen with $\theta_0 = 45°$ before deformation (a, c, e) and at 20% strain (b, d, f): (a, b) (200) plane; (c, d) (020) plane; (e, f) (002) plane. y = compression loading direction; z = plane strain constraint direction.

In order to better determine the mechanism involved in the deformation of the (100)[001] specimens, changes of lamellar and crystal orientation were studied in compression specimens using SAXS and WAXS pole figure techniques. In what follows we introduce a new notation for the coordinate axes of the textured specimens subjected to tension, compression, or simple shear, to differentiate the new axes of testing from the notation used in the channel-die plane strain compression problem that has produced the initial texture. This x–y–z coordinate system is shown in the inset of Figure 12. In this system the y-axis is always the loading direction of the new experiment. Specimens with initial orientations of $\theta_0 = 15°$, 45°, and 75° were selected as representative of the various deformation behaviors observed: (a) $\theta_0 = 15°$ with (100) shear in a kinking mode; (b) 45° with (100) shear alone; and (c) 75° with (100) shear plus a small amount of transverse deformation along the [010] direction. Figures 9–11 and 12–14 show the results of the WAXS pole figure and SAXS studies, respectively.

Figure 9 for the sample with $\theta_0 = 15°$ indicates that during deformation the pole of the (002) plane (i.e., the c-axis) moves away from the loading direction (Figure 9e,f) while remaining in the x–y plane (initial orientation of the (010) plane); the plane including the a- and b-axes, i.e., (200) and (020) poles, rotates toward the loading direction (Figure 9a,b;c,d). The relative positions of the (200) and (020) poles in their common plane do not change. Parts a, c, and e of Figure 9 show the initial orientations of the (200), (020), and (002) poles relative to the compression axis (indicated as y, while parts b, d, and f of Figure 9 show the final orientation of the (200), (020), and (002) poles relative to the compression axis (again indicated as y in the figure) after 20% of compressive strain, respectively. Figure 12 shows the results of SAXS investigations of the deformation of the 15° sample. If the specimen is viewed along the plane strain constraint direction, z, and normal to the loading (y) and transverse (x) directions (see inset Figure 12), we observe from Figure 12a,b that the rotation of the lamella normal, n, is distinctly away from y. When viewed along the transverse direction (x; primary beam normal to z and y), no significant changes of lamellar orientation are observed (see Figure 12c,d). This means that the lamellar normals rotate around the b-axis (see inset of Figure 12) away from the loading direction (y), during the deformation. The SAXS patterns do not change substantially after unloading the specimen. Rotation of both the chain axis, c, and the lamellar normal, n, away from the compression direction is indicative of a kinking type response which should be expected at these small orientation angles. Taking all observations into account, we conclude that the mechanism involved in deformation of the (100)[001] specimen with $\theta_0 = 15°$ is primarily in the form of kinking by means of (100)[001] chain slip and that the kink band is formed by (100)[001] chain slip. The final stages of deformation inside the kink band, monitored by WAXS, show rotation of the c-axis away from the compression direction and the axis n toward it, which confirms that deformation is indeed by fine chain slip inside the kink band.

The X-ray study of the deformation of (100)[001] specimens with initial orientation $\theta_0 = 45°$ shows that the chain axis c rotates away from the compression direction, y, around the b-axis, as in the case of $\theta_0 = 15°$, illustrated in Figure 10a,c,e for the unstrained sample and in Figure 10b,d,f in the sample compressed by 20%. The lamellar normal, n, in turn rotates toward y, as shown in the SAXS

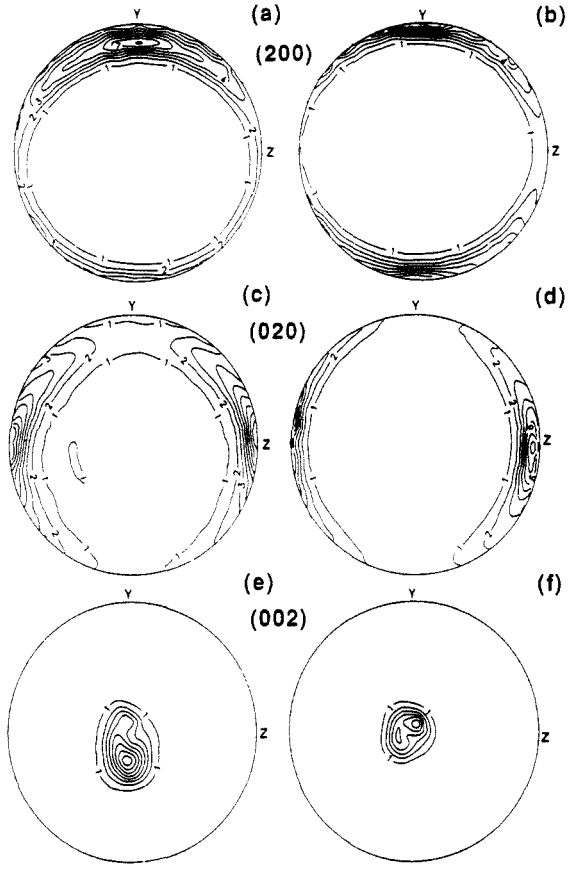

Figure 11. Pole figures of the (100)[001] compression specimen with $\theta_0 = 75°$ before deformation (a, c, e) and at 20% strain (b, d, f): (a, b) (200) plane; (c, d) (020) plane; (e, f) (002) plane. y = compression loading direction; z = plane strain constraint direction.

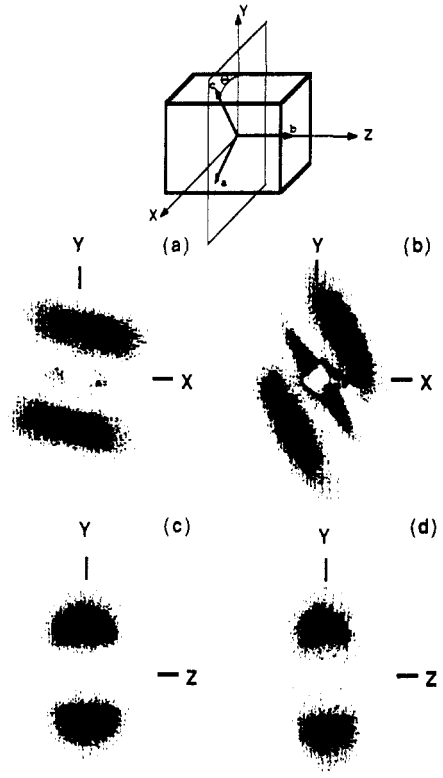

Figure 12. SAXS pattern of the (100)[001] compression specimen with $\theta_0 = 15°$ before deformation (a, c) and after 20% strain (b, d). For a and b the incident beam is parallel to the plane strain constraint direction z; for c and d the incident beam is parallel to the transverse direction x. All directions are as defined in the inset of the figure.

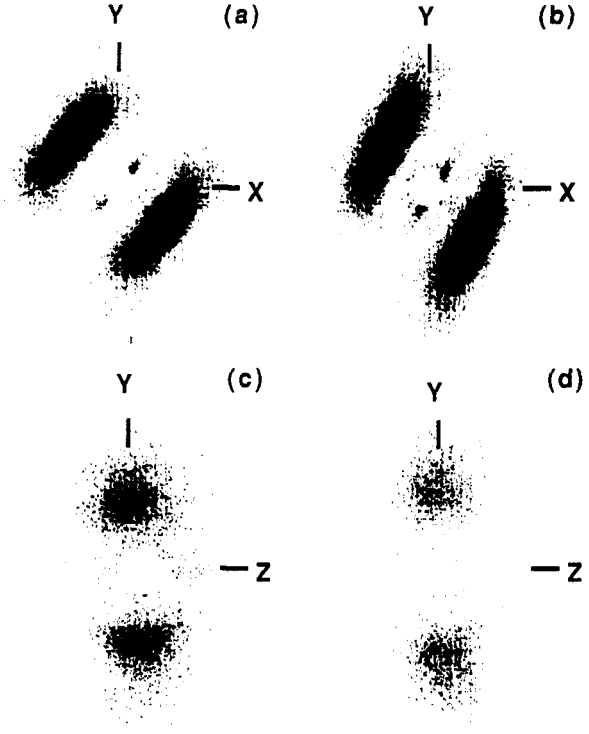

Figure 13. SAXS pattern of the (100)[001] compression specimen with $\theta_0 = 45°$ before deformation (a, c) and after 20% strain (b, d). For a and b the incident beam is parallel to the plane strain constraint direction z; for c and d the incident beam is parallel to the transverse direction x. See the inset of Figure 12 for definition of the directions.

patterns of Figure 13a–d. Such rotations are consistent with (100)[001] fine chain slip being the single deformation mechanism involved.[7] Half-widths of the (200) and (020) diffraction peaks change only slightly with deformation, suggesting relatively stable crystal sizes in the 45° samples.

Examination of the compression-induced texture changes of (100)[001] specimens with $\theta_0 = 75°$ indicates that the chain axis c still rotates away from the loading direction y but does not remain in the y–x plane as was the case of the 15° and 45° samples; the c-axis now tilts slightly toward the constraint direction z (see the WAXS patterns of Figure 11a–f). This new c-axis orientation is a result of the superposition of a rotation around the b-axis and a smaller rotation around the a-axis. The lamellar normal, n, also still rotates toward the loading direction (see the SAXS patterns of Figure 14a,b). Because the high initial orientation angle θ_0, it was difficult to obtain clear SAXS patterns viewing the compressed sample in the transverse direction; thus, it was not possible to determine whether rotation of lamellae proceeded exactly around the b-axis or around some other axis oblique to b. Both WAXS and SAXS data, Figures 11 and 14, respectively, suggest that the 75° specimens deform in compression by (100)[001] fine chain slip as the main deformation mechanism but at least one additional mechanism is also active, which is probably slip on the (010)[001] system. (We recall the previously mentioned fracture surfaces in the compressed specimens with $\theta_0 > 70°$, which are closer to the (010) plane than to either the (100) or (110) planes.) However, the X-ray data, as well as examination of dimensional changes of the specimens after compression, suggest that the activity of this second deformation mechanism is not very strong and that the (100)[001] fine chain slip remains the leading deformation mechanism.

The examination of SAXS data obtained for all three initial orientations shows that deformation by compression does not induce any significant change in the long period (ca. 335 Å). This observation together with results

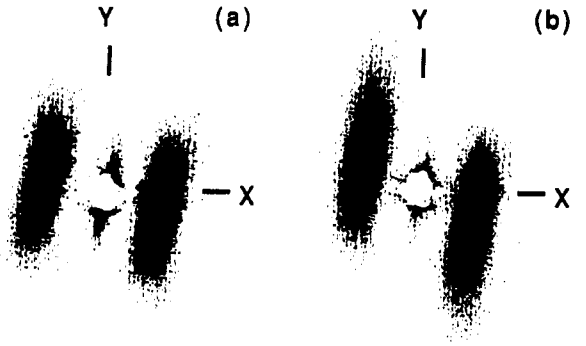

Figure 14. SAXS pattern of the (100)[001] compression specimen with $\theta_0 = 75°$ before deformation (a) and after 20% strain (b). The incident beam is parallel to the plane strain constraint direction z in both cases.

concerning the rotations of n and c suggests that deformation of the amorphous regions (as, e.g., interlamellar sliding) does not occur to any significant extent beyond what compatible deformation with lamellae necessitates in any of the specimens or, at most, is too small to be detected by X-ray techniques. Therefore, we conclude that the deformation mechanisms acting in the crystalline phase are dominant in compression tests of the pretextured material.

On the basis of the results reported above, we conclude further that, in the compression samples for which the geometry was designed to promote (100)[001] chain slip, this mechanism is in fact the dominant deformation mechanism. Moreover, for compression specimens with initial orientation angles in the range of 25–70°, (100)[001] fine chain slip is essentially the single active mechanism. Formation of kink bands for $\theta_0 \leq 20°$ by chain slip is expected and occurs, perhaps even aided by the microvoids mentioned earlier. When θ_0 is small, the resolved shear stress for (100)[001] slip is not high enough to activate chain slip uniformly over the whole crystal but can be sufficient to do so in regions of orientational nonuniformities or in the vicinity of microvoids to cause the initiation of the kink band instability. For larger θ_0 the resolved shear stress in (100) planes for a given external stress is higher than in the case of small θ_0, and initiation of slip does not produce an instability. Therefore, slip is uniform over the entire crystal.

In the case of tension experiments most of the specimens showed brittle behavior. The fracture surfaces were very close to the (100) plane which suggests that the fracture is caused by a structural weakening that is most likely related to the microvoids located in (100) planes of the highly textured HDPE. Those few specimens ($\theta_0 < 20°$) that did exhibit yielding fracture at low strains along the same (100) plane. It is possible to suggest that just before fracture these specimens ($\theta_0 \leq 20°$) also deformed plastically by (100)[001] slip similar to the compression specimens to initiate the fracture process. However, there is no clear evidence for such slip.

Figure 15a,b shows the yield stresses of the (100)[001] specimens calculated from the stress–strain curves using the 4% offset yield definition, plotted against the initial orientation angle θ_0. Also shown in Figure 15a are the stresses at break for brittle tensile specimens. Additionally, the ranges of activity of the various deformation mechanisms are marked. The yield data were used to examine the appropriateness of the Coulomb yield criterion for describing plastic deformation of polyethylene crystals by (100)[001] chain slip. The Coulomb yield criterion has the form

$$\tau = \tau_c - k\sigma_n \tag{1}$$

where τ is the shear stress resolved in the shear plane, σ_n is the resolved stress normal to the shear plane, k is a constant, and τ_c is the critical resolved shear stress required to activate the slip system in question in simple shear. If a material obeys the Coulomb yield criterion, the yield condition reduces to a straight line with the slope $-k$ in τ vs σ_n coordinates. For uniaxial tension or compression under an applied stress σ of the sample in which slip occurs on a plane whose normal makes an angle ξ with the loading direction and for which the angle between the slip direction and loading direction is ϕ (see Figure 31 in the Appendix), the resolved shear stress is given by

$$\tau = \sigma \cos \xi \cos \phi \tag{2}$$

For the geometry employed here, $\xi = 90° - \theta$ and $\phi = \theta$, where θ is the angle between the loading direction and the direction of the chain axis c; hence

$$\tau = \sigma \sin \theta \cos \theta \tag{3}$$

The normal stress can be expressed similarly as

$$\sigma_n = \pm\sigma \cos \xi \sin \theta = \pm\sigma \sin^2 \theta \tag{4}$$

and is positive for any applied tensile stress and negative for applied compressive stress.

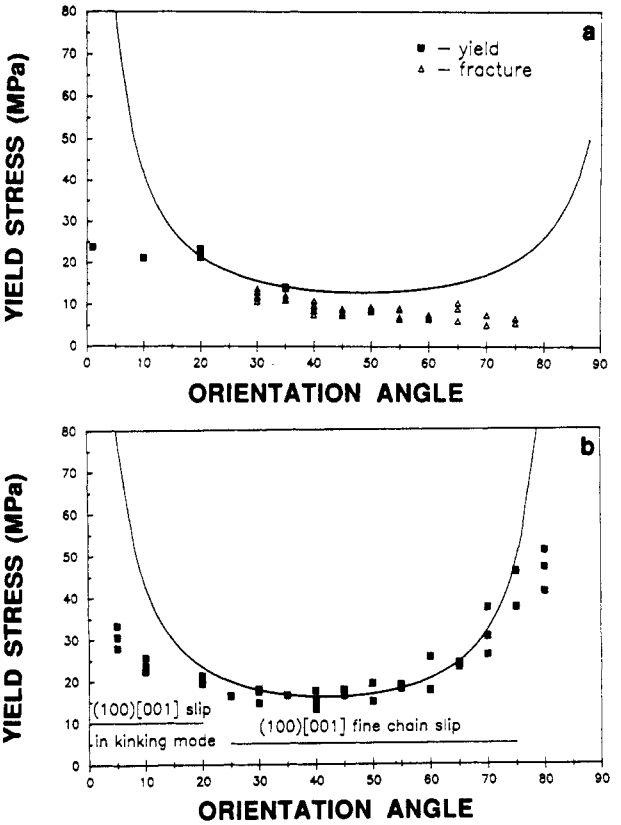

Figure 15. Dependence of the yield and fracture stresses on the initial orientation angle, θ_0, in the (100)[001] specimens deformed in (a) tension and (b) compression.

Using eqs 3 and 4, the shear stress and normal stress were calculated from the yield (and fracture) data shown in Figure 15. These values are presented in Figure 16; for clarity only the average values of stresses at yield for each sample orientation were plotted. Additionally the shear stress determined from the simple shear experiments is also plotted. The geometry of the simple shear specimens permitted obtaining the shear resistance on the (100) plane in the [001] direction directly, since in this case the normal stress, σ_n, is equal to zero, and τ is equal to the measured yield stress. G'Sell[21] found nonzero normal stresses induced in the shear experiments, but the values were small enough to be neglected.

Figure 16 shows that it is possible to fit a straight line to the compression data provided that the fit is limited to

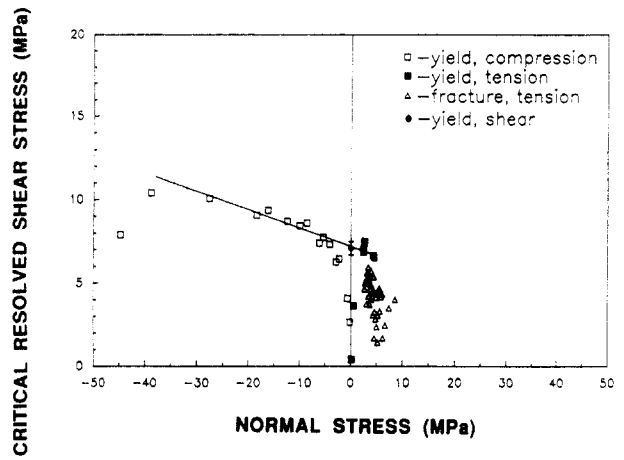

Figure 16. Normal stress dependence of the critical resolved shear stress on the (100) plane in the [001] direction for (100)-[001] specimens.

the range of the initial orientation angle θ_0 of 30–75°, i.e., approximately the range in which (100)[001] fine chain slip is unambiguously active as a single deformation mechanism. That straight line also passes through some of the tensile data as well as data obtained from the simple shear experiments. The best fit values give τ_c = 7.2 MPa and a normal stress coefficient k = 0.11. The determined value of τ_c is within the range estimated by Young et al., 6–10 MPa[1,7] for (100)[100] chain slip at room temperature.

In compression specimens with initial orientation angle $\theta_0 < 30°$ and $\theta_0 > 75°$ as well as in tensile specimens with $\theta_0 < 20°$ the yield occurs at stresses lower than predicted by the Coulomb criterion. In all of these samples, however, competing mechanisms other than the (100)[001] slip process are involved. For small and large θ, according to the Coulomb yield criterion, the yield stress of the raw stress–strain curve for initiating (100)[001] chain slip would have to be very high, so that another deformation mechanism is preferred. Nevertheless, when (100)[001] slip dominates, our results show that the Coulomb yield criterion is an appropriate formulation to describe the yield behavior of polyethylene crystals independent of the type of external stress.

On the basis of the fracture data for tensile specimens presented in Figure 16, we estimate that the value of normal stress at which interfibrillar fracture occurs is about 5 MPa. Such a low value must reflect the effect of the microvoids in the (100) plane. In the absence of such voids the fracture resistance of the material should be significantly higher.

3.3. Deformation by (110)[001] Chain Slip. An attempt was made to determine whether (110)[001] chain slip can be activated using the same experimental procedures. This slip system in polyethylene, although theoretically predicted, has not been observed experimentally. Compression and shear specimens were prepared with orientation and geometry designed to promote (110)[001] deformation. Studies in the tensile deformation mode were difficult because of size limitations of the bar of channel-die oriented material.

The (110)[001] shear specimens fractured at a yield point ($\sigma_y \approx 13$ MPa), but the fracture surface was the (100) plane, forming at 56° angle with the (110) plane. This suggests that the mechanism active before fracture was deformation along the (100) plane, i.e., (100)[001] slip, since this had apparently "precipitated" the brittle behavior also in the (110)[001] samples. The shear stress calculated for the (100)[001] system from the yield data gives a value close to 7.2 MPa, the value of the critical shear stress determined for (100)[001] chain slip. Thus, we conclude that in this experiment the active deformation mechanism was (100)-[001] chain slip instead of the expected (110)[001] slip system or that the shear resistance of the (110)[001] is too high to be probed before reaching a critical condition in the (100)[001] system.

The compression tests suggest a similar deformation behavior of the material. The change of the shape and dimensions of the compressed specimens as well as observed fracture surfaces indicate clearly the strong activity of (100)[001] chain slip, probably as the single active mechanism. Even in the specimens with θ_0 = 45°, where the resolved shear stress for the (110)[001] system reaches a maximum, the deformation proceeds by (100)-[001] slip.

The yield data confirm this behavior. The yield stress, σ_y, for specimens with θ_0 = 45° is 23–24 MPa, which is close to the value of σ_y = 25 MPa expected if the only mechanism active would be (100)[001] chain slip; this value of 25 MPa was estimated for the specimen orientation under consideration, using the previously determined value τ_c = 7.2 MPa for the (100)[001] slip system. Similar estimations performed for other orientation angles (θ_0 = 30–50°) gave similar results; the observed yield stress was close to that expected for deformation by (100)[001] chain slip. For larger θ_0 angles the deformation behavior is affected by fracture along the (100) plane (for which the critical normal stress is only 5 MPa as estimated in the previous section) although some activity of (100)[001] slip can be still observed, which suggests that the fracture is "precipitated" by the shearing of the (100) plane voids. Here too the (110)[001] chain slip seems to be inactive.

For all material orientations examined, no indication was found for (110)[001] chain slip activity. The (100)-[001] chain slip was always found to precede all other deformations. These observations allow us to conclude that (110)[001] chain slip, if possible at all, must have a high critical resolved shear stress, τ_c, for which 13 MPa is a lower bound estimate. We expect that the true critical resolved shear stress for the (110)[001] slip system is in all likelihood significantly higher.

3.4. Deformation by (010)[001] Chain Slip. Studies similar to those described in section 3.2 were conducted on the (010)[001] specimens, i.e., specimens for which the orientation and geometry were arranged to promote plastic deformation by (010)[001] chain slip only. Figure 17 shows typical stress–strain curves obtained from tension (a), compression (c), and shear (b) tests. For all types of externally applied stress the (010)[001] specimens deformed plastically up to large strains. The only relatively brittle behavior was in the tensile specimens with $\theta_0 >$ 75°, for which fracture occurred at or before yield.

The shape of the stress–strain curves for tensile specimens does not change substantially with orientation. In samples with θ_0 up to 60°, strain hardening begins after yield and practically no load drop can be observed. For $\theta_0 < 30°$ the slope of the region of the stress–strain curve corresponding to initial stages of plastic deformation is higher than for θ_0 in the range 35–70° where the slope is smaller. For larger θ_0 a clear maximum in the stress–strain curve can be seen, and the samples break before any strain hardening starts. The elongation at break decreases with the increase of θ_0 above 60°. Finally the specimens break at or before yield for $\theta_0 > 75°$.

Tensile specimens formed deformation bands inclined to the load direction at angles close to θ_0. The angle ω between the deformation band and y was somewhat larger than θ_0 for small θ_0; the difference between ω and θ_0 for θ_0 = 10° was about 10°, and for θ_0 = 30° it was less than 1°. For larger θ_0 the deformation band was inclined to the load direction at an angle lower than θ_0; the initially small

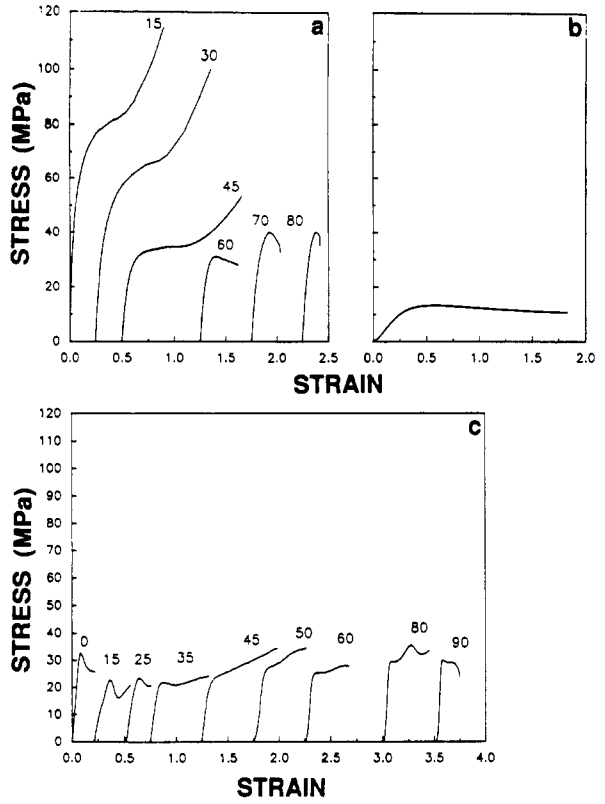

Figure 17. Typical stress–strain curves for (010)[001] specimens tested in (a) tension, (b) shear, and (c) compression. Numbers next the stress–strain curves indicate the magnitude of the angle θ_0 between the initial direction of the chain axis and the direction of tension or compression.

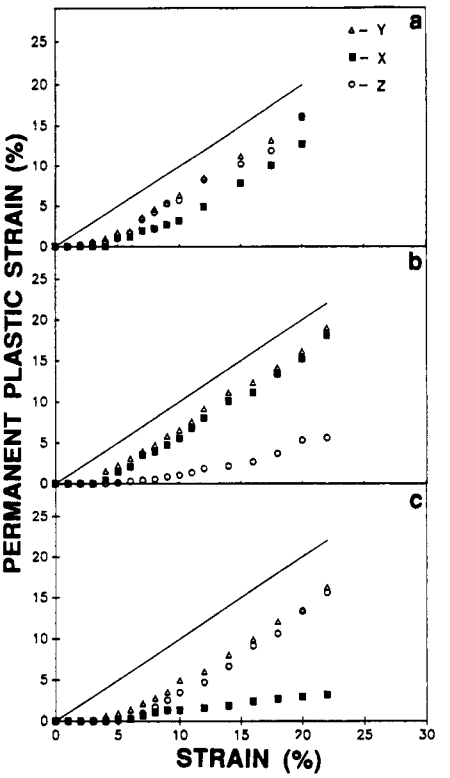

Figure 18. Change of dimensions of (010)[001] compressive specimens as a function of the imposed axial compression strain for the orientation angles (a) 15°, (b) 45°, and (c) 75°.

mismatch between θ_0 and ω increased with increasing strain. The edges of these bands were more diffuse for $\theta_0 < 30°$ and became sharper for larger θ_0, finally resembling the slip bands observed in oriented HDPE of Keller and Rider.[5] Inside the deformation bands, especially those formed in specimens with $\theta_0 < 30°$, some whitening of the polymer was observed, suggesting some form of deformation-induced cavitation inside the band. The above observations suggest that deformation of the tensile specimens might proceed by slip on the (010) plane in the [001] direction when θ_0 is in the range 30–70°. It is very probable that it was the fracture of the lamellae along (100) planes followed by sliding of the smaller blocks that results from this along this plane in the [001] direction. Such a mechanism was referred to as "coarse" chain slip in the literature.[12]

The stress–strain curves for simple shear on the (010)-[001] system, shown in Figure 17b, exhibit a flat maximum near a shear strain of 0.5. No strain hardening is observed. However, at large strains the specimens deform inhomogeneously at their ends, finally fracturing parallel to the shear plane. This behavior undoubtedly influenced the shape of the stress–strain curve at higher strain. The end effects were not observed in initial stages of deformation where the yield stress was determined.

The stress–strain curves obtained from the compression tests, presented in Figure 17c, show a larger variety of shapes than in the tensile experiments. For $\theta_0 < 35°$ there is a significant load drop followed by strain hardening, somewhat characteristic of a kinking response. For θ_0 in the range 35–55° the curves do not show any maximum, and after yielding the stress increases steeply with increasing strain. For $\theta_0 \geq 60°$ the character of the curves changes again; soon after yield the slope of the curve is not too large but increases with increasing strain. The stress drops and subsequently increases again with increasing strain (see the curve for $\theta_0 = 80°$ in Figure 17c). The changes in shape of stress–strain curves correlate with observations of specimens during their compression. In the range of small and medium orientation angles the specimens deform mainly by shear along the (010) plane in the [001] direction, although for small orientation angles there is a noticeable deformation in the [100] direction normal to the shear. For large θ_0 the desired shear in the (010) plane can be seen, but it is not the main deformation mechanism; the greatest change of specimen size is observed in the [100] direction. Specimens with large values of θ_0 often fractured along surfaces close to the (100) plane.

Detailed examinations of the changes in specimen dimensions during compression were carried out for specimens with $\theta_0 = 15°$, 45°, and 75°. The specimen under consideration was compressed to a certain strain and unloaded, and its dimensions were then measured. Then it was compressed again, to a larger strain, and the measurements of shape were repeated. The cycle was repeated up to strains near 20%. For comparison, specimens with the same orientation and size were compressed to a final value of 20% strain in one step, and these showed no significant differences in sample dimensions from those observed in the stepwise compressions. Results are shown in Figure 18. Permanent (plastic) deformation starts for all specimen orientations near an applied strain of about 4–5%. In the specimen with $\theta_0 = 45°$ the relative increase of the specimen width (in the transverse deformation direction, x) is close to the relative decrease of its height (loading direction, y), whereas the change in thickness in the plane strain constraint direction (z) was small but significantly larger than in the case of the (100)[001] specimens. Specimens with $\theta_0 = 15°$ and 75° deformed differently: the relative increase of size along the z direction was larger than along the x direction, especially in the specimen with $\theta_0 = 75°$. The above results indicate that the intended plane strain geometry of the specimens did not always constrain the plastic deformation

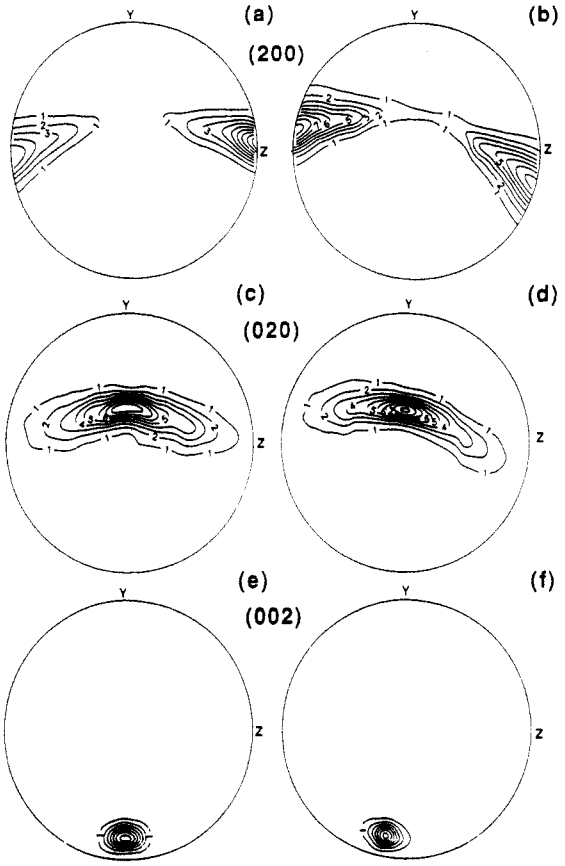

Figure 19. Pole figures of the (010)[001] compression specimen with $\theta_0 = 15°$ before deformation (a, c, e) and after 20% compressive strain (b, d, f): (a, b) (200) plane; (c, d) (020) plane; (e, f) (002) plane. y = compression loading direction; z = plane strain constraint direction. For definition of the directions see the inset of Figure 12.

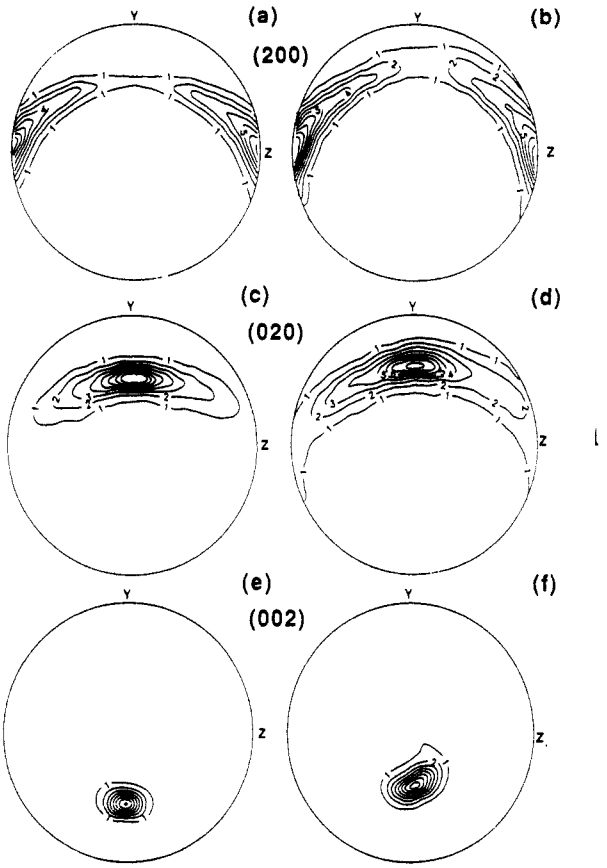

Figure 20. Pole figures of the (010)[001] compression specimen with $\theta_0 = 45°$ before deformation (a, c, e) and at 20% strain (b, d, f): (a, b) (200) plane; (c, d) (020) plane; (e, f) (002) plane. y = loading direction; z = constraint direction.

in directions perpendicular to (010)[001] slip. The (010)-[001] slip mechanism is active in deformation of specimens with θ_0 around 45°, but it is clear from Figure 18 that there is at least one other active mechanism. The situation is more complicated in specimens with low and high θ_0 in which the deformation mechanism(s) causing the increase of specimen thickness along the z direction is/are more active and may actually dominate the deformation. Nevertheless, deformation on the (010)[001] system does indeed take place.

In order to identify the active deformation mechanisms of the (010)[001] compression samples, WAXS and SAXS studies were carried out using techniques analogous to those reported above. Additionally, the crystal and lamellar reorientations in tensile specimens were studied by WAXS and SAXS, respectively, but the use of the pole figure technique was very difficult because of the small size of the tensile specimens. Therefore, only two-dimensional WAXS patterns were recorded for tensile specimens. Results are presented in Figures 19–25.

During compression of the (010)[001] specimens with $\theta_0 = 15°$ and 45° the chain axis c (the pole of the (002) plane) moves away from the loading direction and the common plane of (200) and (020) poles moves toward it. This is shown in Figure 19a–f for the $\theta_0 = 15°$ sample and in Figure 20a–f for the $\theta_0 = 45°$ sample. The axis of rotation of the crystallites is inclined to the initial a-axis, and the rotation can be considered as a superposition of rotations around the initial a- and b-axes (see inset on Figure 22). The rotation around the b-axis is larger in the 15° specimens than in the 45° specimens. SAXS results (Figures 21 and 24) show that the rotation of the lamellar normal, n, is also a superposition of two rotations: (i) around the a-axis toward the loading direction if $\theta_0 = 15°$ and away from it, if $\theta_0 = 45°$, and (ii) around the b-axis, away from the loading direction. These rotations of the chain axis, c, and lamellar normal, n, can be interpreted in both cases of specimen orientation as a result of superposition of two mechanisms acting simultaneously. Of these, one is (010)[001] chain slip (which in the case of $\theta_0 = 45°$ results in rotation of c away from the compression direction and n toward it, both around the a-axis, indicating homogeneous deformation, and in the case of $\theta_0 = 15°$ results in the rotation of c and n together around the a-axis, away from the compression direction, indicating kinking or "coarse" slip; and the second is (100)[001] chain slip, in a kinking mode, where both c and n rotate together around the b-axis away from the loading direction.[7] An alternative explanation for the observed rotations of the c- and n-axes which might be proposed is that the second deformation mechanism active was not (100)[001] but (110)[001] chain slip in a kinking or coarse slip mode. The occurrence of such slip together with (010)[001] chain slip would cause the rotation of c- and n-axes similar to those described above. The values of the angles of rotation of c and n indicate that the slip on the second system ((100)-[001] or (110)[001]) is more active for the specimen with $\theta_0 = 15°$ than for that with $\theta_0 = 45°$. Examination of the width of the respective diffraction peaks showed about a 10% decrease of the average dimension of crystallites in the [100] direction after deformation, similar in magnitude to the decrease of the crystal size in the [010] direction in the sample with $\theta_0 = 15°$. There was almost no change of crystal size in the [010] direction for samples with $\theta_0 = 45°$. This observation additionally confirms the fine character of (010)[001] slip for $\theta_0 = 45°$ and its kinking mode character for $\theta_0 = 15°$. It would also suggest that the second mechanism that is active is (100)[001] chain

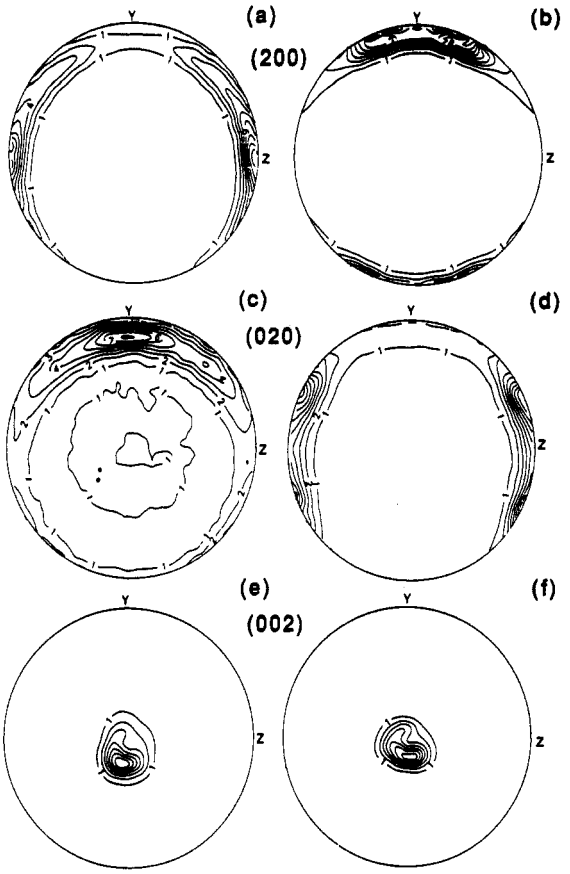

Figure 21. Pole figures of the (010)[001] compression specimen with θ_0 = 75° before deformation (a, c, e) and after 20% compressive strain (b, d, f): (a, b) (200) plane; (c, d) (020) plane; (e, f) (002) plane. y = loading direction; z = constraint direction.

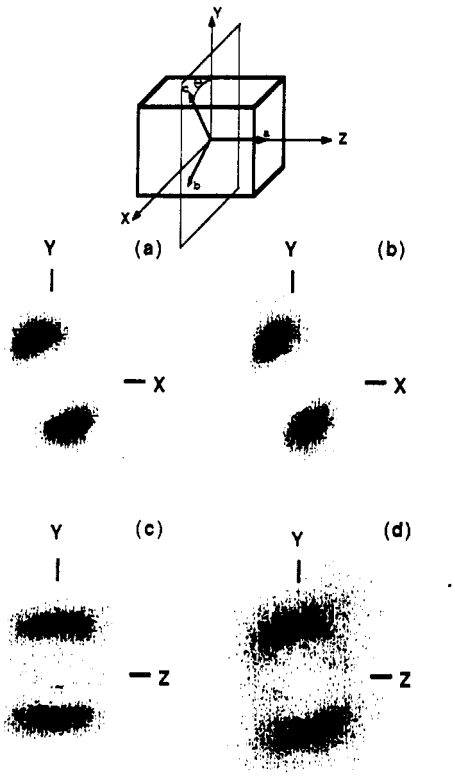

Figure 22. SAXS pattern of the (010)[001] compression specimen with θ_0 = 15° before deformation (a, c) and after 20% compressive strain parallel to constraint direction z; (c, d) incident beam parallel to transverse direction x. y = loading direction; x = transverse (free) direction; z = plane strain constraint direction, as defined in the inset figure.

slip rather than (110)[001] chain slip, both in a kinking mode, because in the latter case the crystallite size should

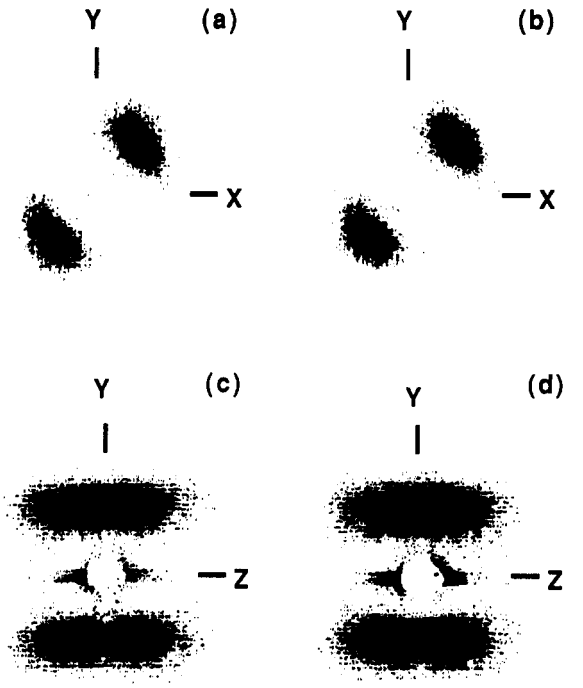

Figure 23. SAXS pattern of the (010)[001] compression specimen with θ_0 = 45° before deformation (a, c) and after 20% compressive strain (b, d): (a, b) incident beam parallel to constraint direction z; (c, d) incident beam parallel to transverse direction x. Directions are defined in the inset of Figure 22.

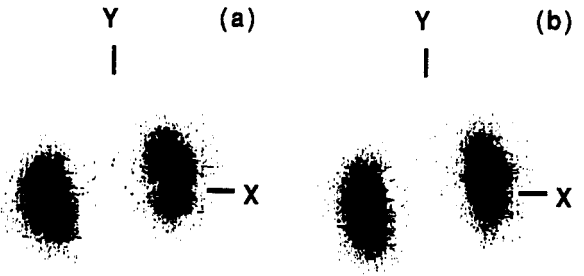

Figure 24. SAXS pattern of the (010)[001] compression specimen with θ_0 = 75° before deformation (a) and after 20% compressive strain (b); incident beam parallel to constraint direction z in both cases. Directions are defined in the inset of Figure 22.

be influenced in both [100] and [010] directions. That was not the situation for specimens with θ_0 = 45° in which the crystallite size in the [010] direction remained undisturbed.

Studies of (010)[001] specimens with θ_0 = 75° revealed a completely different behavior than described above. The chain axis, c, rotates around the initial a- and b-axes away from the loading direction, while the poles of (200) and (020) planes change position in their common plane; each pole splits in two, and the angle between the old and new position of the poles is close to 67° (see Figure 21b,d). This indicates quite clearly that the (110) and (1$\bar{1}$0) twinning modes were active during compression of the 75° specimens.[14] The poles of (200) and (020) planes appear in new positions in early stages of the compressive deformation, but there is still a large fraction of untransformed crystals. The spatial distribution of poles shows maxima in the old (before compression) and new (after twinning) positions. With increasing strain the maxima in the old positions slowly disappear, and finally only those in the new positions are visible. These observations suggest that twinning was initiated locally in the sample and spread over the sample with increasing strain. Rotation of the c-axis away from the loading direction suggests that, besides twinning, crystallographic slip was also active. The lamellar normal, n, rotates toward the loading direction

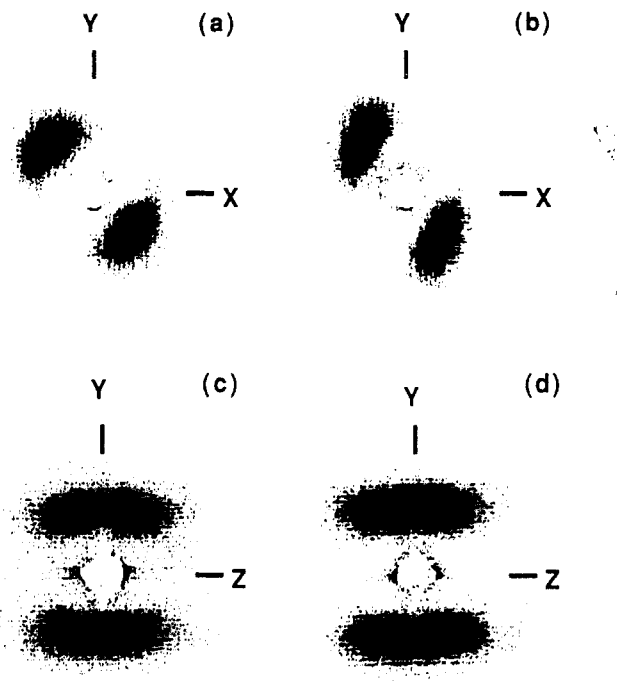

Figure 25. SAXS pattern of the (010)[001] tensile specimen with $\theta_0 = 45°$ before deformation (a, c) and after 20% tensile strain (b, d): (a, b) incident beam parallel to constraint direction z; (c, d) incident beam parallel to transverse direction x. Directions are defined in the inset of Figure 22.

as the SAXS patterns of Figure 24a,b show. However, it is difficult to distinguish whether slip took place in the untwinned or twinned crystals. Consideration of crystallite orientation suggests that, before twinning, (010)[001] slip was favored, whereas in the twinned crystals (100)[001] slip apparently is easier (see Figure 32 in the Appendix). Both slip systems were probably active, similar to the specimens with lower θ_0. Moreover, in twinned crystals the (100)[010] transverse slip may be relatively easy (cf. Figure 32d in the Appendix). However, observed rotations of crystallographical axes do not confirm its activity, so it is probably less active than the chain slip systems.

SAXS patterns of the tensile (010)[001] specimens with $\theta_0 = 45°$, in Figure 25a–d, show that during specimen elongation the lamellar normal, n, rotates around the a-axis toward the loading direction; there is no rotation around b. The WAXS patterns (not shown) indicate rotation of the a-axis toward the loading direction, which implies rotation of the chain axis, c, away from the loading direction. The results suggest that deformation occurs by (010)[001] fine chain slip in the absence of either (100)[001] or (110)[001] slip.

To summarize, the deformation behavior of (010)[001] specimens occurs as follows: In compression experiments, when the initial angle is small $\theta_0 \leq 25°$ and kinking should be expected, (010)[001] chain slip appears to occur in a kinking mode, and (110)[001], or more probably, (100)[001] chain slip, again in a kinking mode, is also active as a second mechanism. Activity of the latter slip system was not expected due to the orientation of (100) planes being parallel to the loading direction and additionally because of the relatively large dimension of the sample in the [100] direction acting as the plane strain constraint direction. However, because the orientation of crystallites in the sample is not perfect, there is a significant fraction of crystallites whose (100) planes are somewhat inclined to the loading direction, some even at reasonably large angles. On these particular planes, the resolved shear stress for (100)[001] slip is high enough to produce slip and initiate a kinking mode of deformation. Because of the presence of microvoids in the (100) planes the kinking process can be aided further to activate this type of response sooner. A similar situation was discussed for the deformation of (100)[001] specimens with low initial orientation angles, in section 3.2. On the other hand, the second active slip system in compression specimens could be (110)[001] chain slip instead of (100)[001], the possibility of which was discussed above. For specimen orientations that were studied here the Schmid factor for (110)[001] slip system is only 20% lower than the Schmid factor for the (010)[001] chain slip studied, independent of the orientation angle θ_0. This makes the (110)[001] slip relatively easy to activate as a second mechanism, provided that the critical resolved shear stress for this slip system is indeed lower or equal to the critical resolved shear stress for the (010)[001] slip system. In the previous section we estimated the lower limit for τ_c for (110)[001] chain slip to be 13 MPa. Taking into account that estimate and the value $\tau_c = 15.6$ MPa for (010)[001] slip (see below), one can estimate that the compressive stress necessary to induce plastic deformation by (110)[001] slip may be only several percent higher than that necessary to initiate (010)[001] slip. Thus, (110)[001] chain slip, again in a kinking mode, seems to be a very reasonable possibility for a second deformation mechanism observed in the specimens considered here. However, we repeat the fact that (110)[001] chain slip has never been detected experimentally, even in the carefully designed experiments discussed earlier. Moreover, the "activity ratio" of (010)[001] and the possible (110)[001] slips should not depend on θ_0 as does the ratio of Schmid factors for both systems. The experimental results show, however, that the relative activity of a second, minor mechanism increases with a decrease of θ_0. Such behavior could be explained if the (100)[001] chain slip was assumed as a second active mechanism (see below).

For θ_0 in the range 30–60°, where stable homogeneous slip behavior becomes possible, (010)[001] fine chain slip appeared to be the main deformation mechanism. A kinking type of response by a second system appeared still active, although it was weaker than in the case of specimens with lower θ_0, as might be expected. If the second mechanism is (100)[001] chain slip in a kinking mode, then its relatively lower activity in specimens with mid-range values of θ_0 may arise from the fact that the resolved shear stress for the (100)[001] system depends critically on the angle of local variation of orientation inside the specimen and relatively less on θ_0, whereas the resolved shear stress for the (010)[001] system increases markedly with θ_0, increasing from 0 to 45°. This increase makes (010)[001] slip easier with increasing θ_0. Thus, (010)[001] dominates in the range θ_0 near 45°, regardless of the identity of the second competing mechanism.

When the angle θ_0 increases above about 60–70°, another mechanism becomes active. At such orientations the resolved shear stress for the (010)[001] system again decreases so this slip system is more difficult to activate than for the case of θ_0 in the 30–60° range. On the other hand, the shear stress resolved in the (110) plane in the [110] direction (as well as in the (110)[110] system) becomes high enough to activate {110} twinning modes for which τ is proportional to $\sin^2\theta$, whereas for chain slip it is proportional to $\sin\theta\cos\theta$ (see the Appendix). The critical resolved shear stress, τ_c, for {110} twinning, was estimated to be 14.5 MPa[13] and is close to τ_c expected for (010)[001] chain slip (15–17 MPa,[7,17] 15.6 MPa as found in the present study), so competition between these two mechanisms is expected. As a result, {110} twinning modes become the main mechanism active in deformation of specimens with large angles θ_0. Chain slip may be still

active, but plastic deformation starts by twinning. After twinning, further plastic deformation proceeds by the chain slip mechanism. Both of the above-mentioned chain slips are probably involved, but because of the orientation of the twinned crystals the (100)[001] chain slip is probably preferred. One can expect that also (100)[010] transverse slip is active in twinned crystals, but its experimental evidence is weak.

In tensile deformation of specimens with an initial orientation around 45° the (010)[001] chain slip seems to be the only deformation mechanism. Slip on other planes ((100) or (110)) is probably too difficult because of strong constraints imposed by the gripped sample ends (specimens had low aspect ratios). Moreover, there is an additional constraint for (100)[001] slip in tensile deformation. In tensile deformation any slip process causes a rotation of the slip plane normal away from the loading direction.[1] In the present case, the (100) plane normals have an average orientation perpendicular to the loading direction, so the majority of crystallites is already oriented along the loading direction and slip on the (100)[001] system in these crystallites is not possible since the resolved shear stress τ is very small. The (100)[001] slip can start only in those crystallites which have significantly different orientation (locally the angle between the (100) plane normal and the loading direction is less than 90°, so $\tau > 0$). In this case these (100) slip plane normals rotate, becoming perpendicular to the loading direction; the resolved shear stress, being the driving force of that slip system, quickly decreases to a very small value, to stop this slip process. In this way the only slip system remaining to give further plastic deformation is the (010)[001] chain slip system. On the other hand, if we assume the (110)[001] chain slip as a possible second deformation mechanism, then in tensile specimens the only constraints preventing the occurrence of such slip are those imposed by the gripped ends of the specimen. The absence of slip other than (010)[001] chain slip was confirmed by WAXS and SAXS results—neither lamellar nor chain rotation around the *b*-axis was detected, indicating the inactivity of either (100)[001] or (110)[001] chain slip in the tensile deformation mode.

In tensile specimens with larger initial orientation angles, θ_0, the resolved shear stress for (010)[001] chain slip (at a given stress σ) decreases; thus, this slip is more difficult, and the other chain slips are still constrained. On the other hand, the normal stress, σ_n, on the (010) plane increases with θ_0 and finally reaches a critical value for interfibrillar fracture along the (010) plane. As a result, the specimens with $\theta_0 > 80°$ show brittle behavior. In the case of tensile specimens with low orientation angles, the X-ray data and whitening inside the deformation band indicating formation of microvoids may suggest the coarse character of the (010)[001] chain slip.

The deformation behavior of (010)[001] specimens, i.e., the dependence of the yield stress on initial orientation angle, θ_0, is shown in Figure 26a for tension and Figure 26b for compression. In this figure the offset yield stress, determined from stress–strain curves, is plotted as a function of σ_0. On the basis of the above yield data, the resolved shear stress, τ, and normal stress, σ_n, for the (010)[001] system were calculated according to the procedure described in the previous section. Figure 27 presents these stresses (determined from tension, compression, and shear data) in the τ vs σ_n coordinates. It is seen that the dependence of τ on σ_n can be approximated in certain ranges of σ_n by a straight line, supporting the validity of the Coulomb yield criterion (eq 1). The linear regions correspond to the following ranges of initial orientation angles: 30–60° and 25–75° for compression and tension

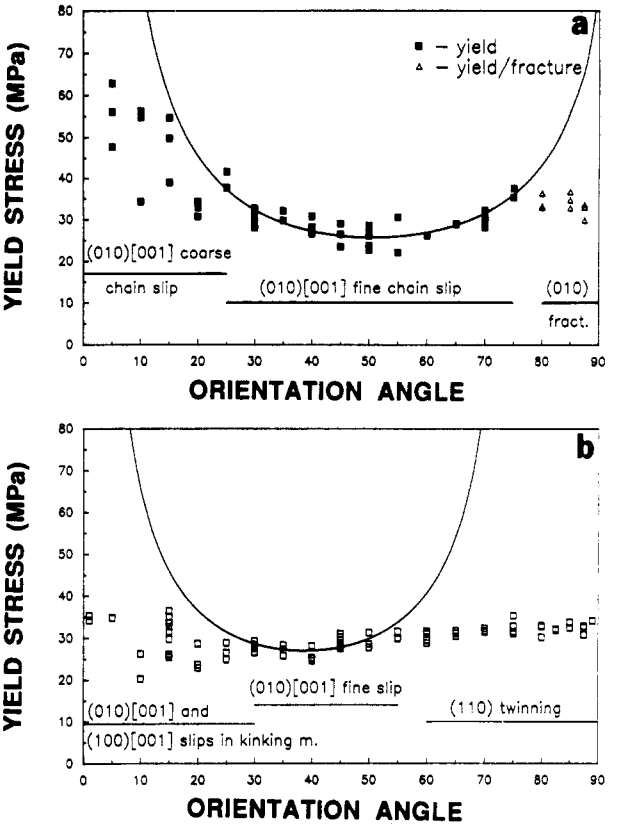

Figure 26. Dependence of yield and fracture stresses on the initial orientation angle, θ_0, in the (010)[001] specimens deformed in (a) tension and (b) compression.

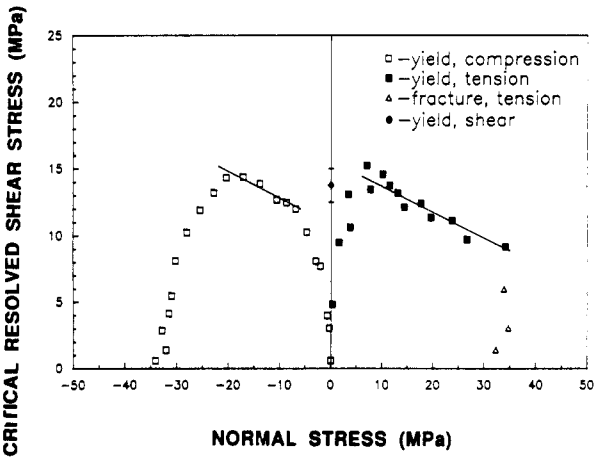

Figure 27. Normal stress dependence of the critical resolved shear stress on the (010) plane in the [001] direction for (010)[001] specimens.

tests, respectively. Thus, these ranges coincide with the ranges of θ_0 in which (010)[001] chain slip is a principal active deformation mechanism. As was discussed above, in other ranges of θ_0 some additional mechanisms are active. Thus, one can conclude that the Coulomb yield criterion is an appropriate yield criterion for (010)[001] chain slip, as it was for (100)[001] chain slip. However, Figure 27 shows that the line determined from compression data has different parameters from the line determined from the tensile data set. The "best fit" values of critical resolved shear stress, τ_c, and the normal stress dependence coefficient, k (see eq (1) are τ_c = 10.79 MPa and k = 0.223 based on the compression data and τ_c = 15.60 MPa and k = 0.193 based on the tension data. To understand these results, it is necessary to take into consideration that in tension (010)[001] fine chain slip is essentially the single active deformation mechanism, since slip should be homogeneous and stable, whereas in compression, par-

ticularly in the small θ_0 range, the (100)[001] chain slip in the kinking mode (or possibly (110)[001] chain slip) also takes place. Thus, one can conclude that the value of τ_c determined from compression yield data is affected by the unexpected activity of the relatively easier (100)-[001] slip process. As was determined in section 3.2, τ_c for (100)[001] chain slip is 7.2 MPa, which is significantly lower than the values determined for (010)[001] slip. (We note that, by assuming that (110)[001] slip is the second mechanism active in compression, the difference in the value of τ_c determined from tension and compression data cannot be explained easily. Even assuming the lowest possible critical shear stress for (110)[001] slip, the estimations do not suggest any decrease of the yield stress in compression, compared to the expected yield stress in the absence of the secondary slip besides (010)[001].) In tension, only the (010)[001] slip system is active, so the value of τ_c = 15.6 MPa determined from tension data is a more reliable and appropriate value for the critical resolved shear stress for (010)[001] chain slip. This value agrees well with τ_c = 15 MPa determined previously by Young et al.[7] and τ_c = 16.6 MPa by Burnay and Groves.[17]

The normal stress dependence coefficients determined from compression and tension data have slightly different values: 0.223 for tension and 0.193 for compression. However, it is possible to fit reasonably well both data sets with straight lines having the same slope $k \approx 0.2$. This fit is reasonable, considering the additional slip on the (100) plane which is active in compression and which depends primarily on the distribution of the local orientation of (100) planes, and its correlation with normal stress on the (010) plane is of less importance. That is, the activity of (100)[001] as a secondary slip mechanism should influence only the value of τ_c and not k.

The above considerations lead to the conclusion that the Coulomb yield criterion with the values $\tau_c \approx 15.6$ MPa and $k \approx 0.2$ is an appropriate yield criterion for (010)[001] fine chain slip in polyethylene crystals. These values are nearly 2 times higher than the corresponding values determined for (100)[001] chain slip, a result that is in accordance with theoretical predictions made on the basis of the consideration of dislocation mobility (see ref 1). Moreover, there is some evidence that (100) is the fold plane in bulk-crystallized samples of polyethylene.[24,25] This should additionally make the (100)[001] chain slip easier to activate.

3.5. Deformation by (100)[010] Transverse Slip. The (100)[010] specimens were cut out from oriented HDPE so that the chain axis, c, was always normal to the loading direction and the (100) plane normal formed the angle θ_0 with the loading direction. These samples were intended for use in the study of the (100)[010] transverse slip system, i.e., as the principal slip mode in a direction normal to the chain axis.

Figure 28 shows the types of stress–strain curves obtained from compression experiments on (100)[010] specimens. In the range of θ_0 = 0–25° the specimens deformed plastically up to strains of about 20% and then fractured. When θ_0 was 30–55° the specimens fractured near the yield point; for $\theta_0 > 60°$ plastic behavior was observed once again with fracture occurring near 10% strain. All tensile specimens for the (100)[010] system showed brittle behavior, fracturing before the yield point. In both compression (θ_0 = 20–70°) and tensile specimens of all orientations, fracture surfaces were parallel to the (100) crystal planes. In the case of tensile specimens, fracture was frequently initiated at the curved edge of the specimen, beyond the gauge area where stress concentrations exist, similar to the behavior of (100)[001] tensile specimens. The orientation of fracture surfaces suggests

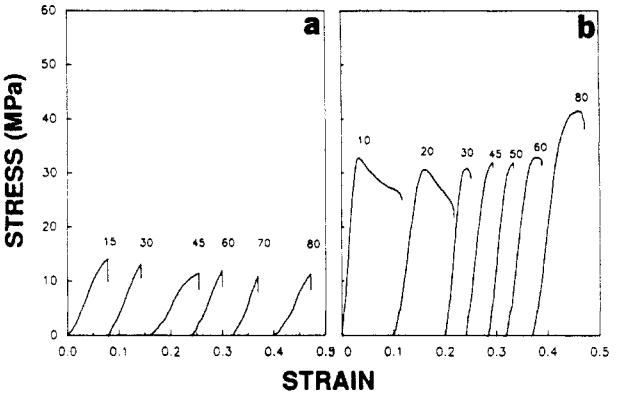

Figure 28. Typical stress–strain curves for (010)[001] specimens tested in (a) tension and (b) compression. Numbers next to the stress–strain curves indicate the magnitude of the angle θ_0 between the initial direction of the chain axis and the direction of tension or compression.

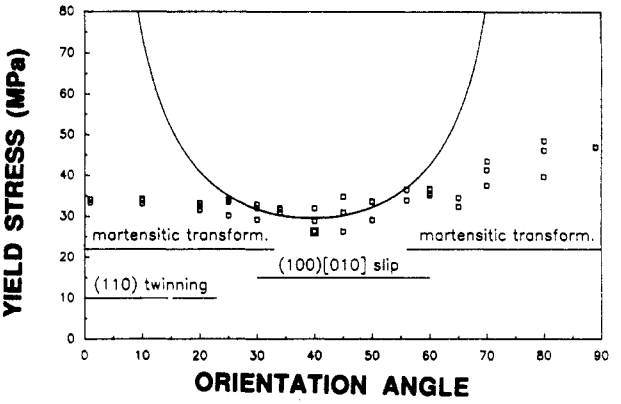

Figure 29. Dependence of yield and fracture stresses on the initial orientation angle, θ_0, in the (100)[010] specimens deformed in (a) a tensile test and (b) a compression test.

that neither (010)[100] nor (110)[1$\bar{1}$0] transverse slip processes were active in any of the tensile specimens studied.

The deformation behavior of samples similar to our (010)[001] compression samples was studied by Young and Bowden.[13] They found that, depending on initial orientation angle θ_0, different deformation mechanisms are active. For small θ_0, up to 30°, (110) twinning combined with a $T1_2$ martensitic transformation are the deformation mechanisms responsible for yielding. For θ_0 in the range of 30–80° (100)[010] transverse slip takes place, being the only mechanism near θ_0 = 45° and combined with $T1_2$ martensitic transformation for other angles. For θ_0 larger than 80° the martensitic transformation alone occurs on loading, and (110) twinning was observed on unloading the sample. Using the Schmid law, the critical resolved shear stresses, τ_c, for these mechanisms were estimated as 14.5 MPa for (110) twinning, 12 MPa for (100)[010] transverse slip, and 14 MPa for $T1_2$ martensitic transformation.[13]

The ranges of activity of the particular transverse mechanisms, determined in ref 13, are marked in Figure 29 where the yield/fracture data obtained in the present study are shown. Figure 30 shows the shear and normal stresses for the (100)[010] transverse slip system. As in the case of chain slips, it is possible to fit a straight line to part of the compression yield data, corresponding to the ideal θ_0 range of 30–55°, i.e., the range in which (100)[010] transverse slip was the dominant deformation mechanism in homogeneous form. The Coulomb yield criterion may, therefore, be used to describe the yield behavior of polyethylene crystals when transverse slip on the (110)-[010] system is the dominant deformation mechanism.

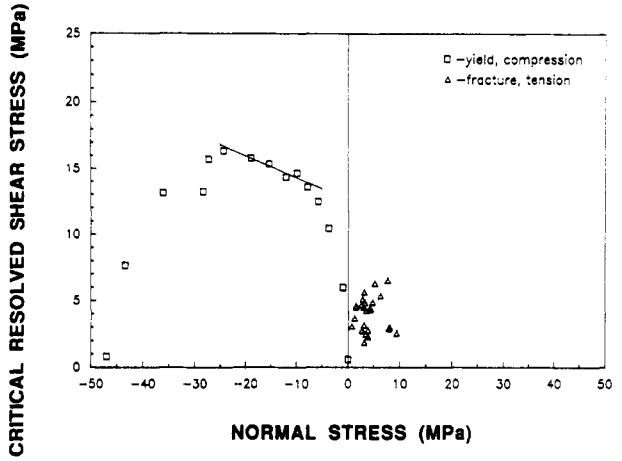

Figure 30. Normal stress dependence of the critical resolved shear stress on the (100) plane in the [010] direction for (100)-[010] specimens.

Table II
Critical Resolved Shear Stress and Normal Stress Coefficients for Slip Systems Studied

slip system	τ_c (MPa)	k
(100)[001]	7.2	0.11
(010)[001]	15.6	0.20
(110)[001][a]	>13	
(100)[010]	12.2	0.17

[a] The τ_c value is the lowest estimate.

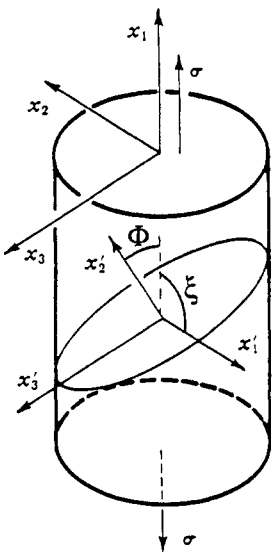

Figure 31. Slip system coordinates for a single crystal under uniaxial tension (or compression).

The best fit value of the critical resolved shear stress, τ_c, is 12.2 MPa and the normal stress coefficient, k, equals 0.17.

The stress–strain curves show that compression specimens that deform by (100)[010] transverse slip fracture quite easily, just near the yield point, suggesting that the deformation is not stable in the course of plastic deformation and, unless it is combined with another mechanism, (100)[010] slip is stifled by precipitating fracture before large plastic strains can develop. Similar behavior was reported by Young and Bowden;[13] thus, this may be a feature of (100)[010] transverse slip itself and may not be connected with the particular morphology of the samples investigated in this study, including the presence of microvoids in the (100) planes in our specimens. Generally, however, the existence of microvoids promotes fracturing along (100), at larger strains, as was discussed in section 3.2. The lack of plasticity associated with the

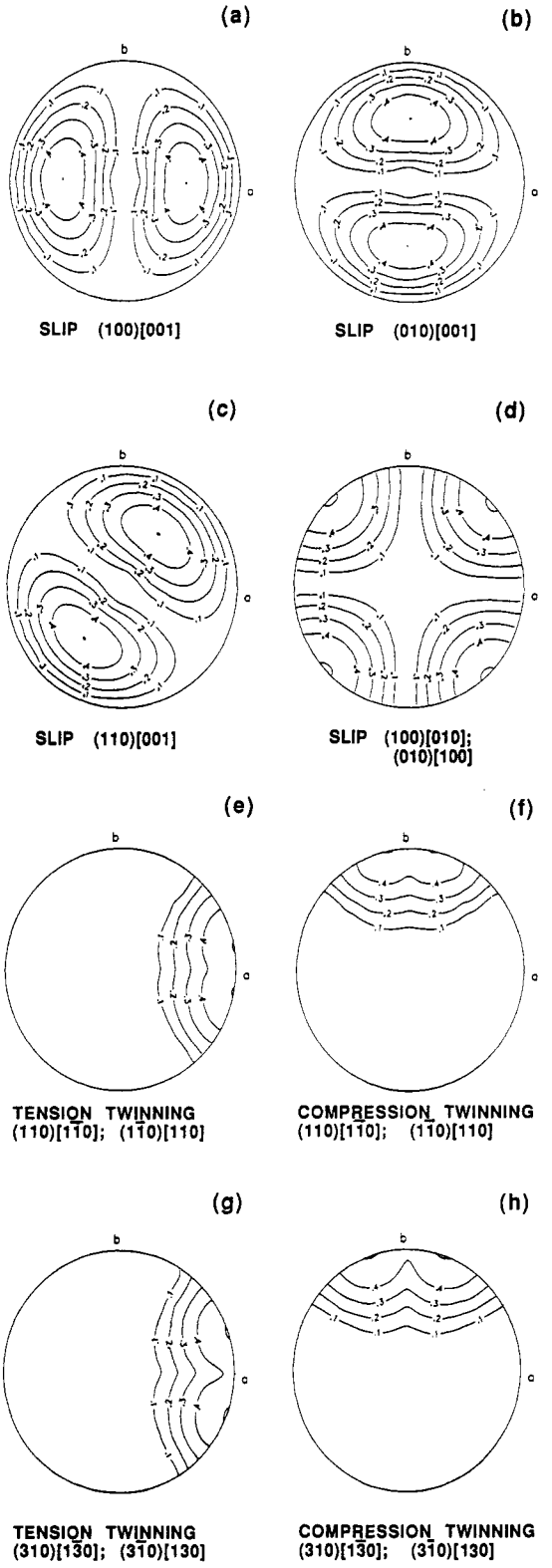

Figure 32. Plots of contours of constant Schmid factor, m (isostress lines), for uniaxial tension or compression in the stereographic projection normal to the [001] crystallographical direction in orthorhombic polyethylene for (a) the (100)[001] chain slip (tension and compression), (b) the (010)[001] chain slip (tension and compression), and (c) the (110)[001] chain slip (tension and compression); the plot for the conjugate ($\bar{1}$10)[001] slip may be obtained by mirror reflection with respect to the (100) plane), (d) the (100)[010] and (010)[100] transverse slips (tension and compression; the Schmid factors for both mechanisms are identical for every load orientation), (e) the (110)[1$\bar{1}$0] and (1$\bar{1}$0)-[110] twinning systems under tension, (f) the (110)[1$\bar{1}$0] and (1$\bar{1}$0)[110] twinning systems under compression, (g) the (310)-[1$\bar{3}$0] and (3$\bar{1}$0)[130] twinning systems under tension, and (h) the (310)[130] and (3$\bar{1}$0)[130] twinning systems under compression. The directions of crystallographic axes **a** and **b** are marked on the plots; the **c**-axis is perpendicular to the projection plane.

(100)[010] transverse slip system may be connected with the fact that the (100) plane is most probably the plane of chain folds in oriented HDPE.[24,25] In such a situation the adjacent (100) planes are not tied together by folded molecules; there are only van der Waals forces between them, and fracture may be quite easy to initiate by a small amount of transverse slip. Note that transverse slip proceeds perpendicular to the chain axis and not along it, so any slip dilatency or presence of orientational variations may enhance the tendency to fracture by the growth of imperfections between planes and result in fracture of the crystal along the (100) plane. The previously mentioned microvoids in the (100) plane are probably responsible here for the brittleness in tension by acting as the imperfections that become accentuated by slip. The normal stress across the (100) plane necessary to initiate the fracture along the (100) plane in tension (as suggested by Figure 29) is close to that observed in the case of (100)-[001] tensile specimens and can be estimated as 5–6 MPa.

The results for all critical resolved shear stresses on active slip planes and their sensitivity to normal stress are summarized in Table II.

The mechanistic implications of the measurements of deformation resistance in this paper will be discussed fully in connection with the results of a separate study of simulation of plastic deformation in semicrystalline polymers by Ahzi et al.[26]

Finally, it is to be noted here that most of the measurements of plastic resistance have been obtained at a single strain rate. Since plasticity is relatively strain rate insensitive, this is not a serious omission. Nevertheless, the effect of strain rate changes during plastic deformation has important mechanistic implications. These are presently under study by Lin and Argon[29] and will be reported elsewhere.

4. Conclusions

Taken overall, the array of experimental results presented here allows us to make some broad and general statements about the deformation of high-density polyethylene. First, it is clear that, regardless of the care taken to construct an appropriately pretextured sample and/or a well-designed specimen geometry, there are usually competing crystallographic deformation mechanisms operating in any mechanical test. With careful monitoring of the changes in orientations of the crystallographic axes through the study of WAXS pole figures *and* the reorientations of the lamellar morphology through the study of 2D SAXS patterns, it is possible to find ranges of specimen orientation in which a single mechanism is the dominant source of strain response to the macroscopic applied stress. Simple observations of the changes in sample dimensions have also been found to be very useful to augment the conclusions drawn from WAXS and SAXS data.

In those narrow regions of deformation in which a single deformation mechanism could be isolated, it was found that the Coulomb criterion gave an adequate description of the yield surface for three mechanisms: (100)[001] chain slip, (010)[001] chain slip, and (100)[010] transverse slip. The critical resolved shear stress, τ_c, and normal stress dependence coefficients, k, for these mechanisms are summarized in Table II. Outside the narrow regions of single mechanism dominance, a wide variety of competing processes was observed, including some fracture processes "catalyzed" by microvoids which exist along the (100) planes of the channel-die pretextured materials. Twinning on the (110) plane was clearly observed in competition with (010)[001] chain slip.

None of our experiments revealed any evidence of (110)-[001] chain slip or (010)[100] or (110)[1$\bar{1}$0] transverse slip. We conclude therefore that the (100)[001], (010)-[001], and (100)[010] mechanisms are the main slip systems involved in the deformation of HDPE, although we cannot exclude completely the activity of (110)[001] chain slip in a very limited range of orientations. The (110) twinning and $T1_2$ martensitic transformation mechanisms may also be active for certain crystal orientations. The quantitative information on the three dominant slip systems studied here is useful and necessary information for definitive models or computer simulations of texture evolution in HDPE. Such a simulation is presented in a separate paper by Ahzi et al.[26] where the mechanistic implications of the present measurements are also discussed.

We made no direct attempt to study the important deformation characteristics of the amorphous fraction of our specimens. In any quantitative model designed to predict or describe the deformation of HDPE, a constitutive law for the amorphous material will be required. The development of such a constitutive law is greatly complicated by the fact that not only the amount of amorphous material but also its detailed topological structure is greatly dependent on thermomechanical history and molecular weight and spatial distribution of the particular HDPE material under study (see, e.g., ref 27). We used only a single HDPE sample which was crystallized and processed according to a single set of procedures. Therefore, the amorphous fraction was essentially a constant, albeit uncharacterized, material in all of our experiments. On the other hand, each of the individual crystalline deformation mechanisms examined here is activated by its critical resolved shear stress, and it responds to normal stress according to the coefficients of the Coulomb yield criterion we have determined, regardless of any changes which might occur from sample to sample in the amorphous material. In this sense, the availability of quantitative mechanistic input on the three important crystalline deformation systems of HDPE leaves only the constitutive law of the amorphous material as the adjustable information in a fully descriptive model of the deformation of HDPE. To the extent that other future studies can better characterize the structure and mechanical properties of the amorphous content of HDPE, this last element of empiricism can be reduced or eliminated. Moreover, all the existing evidence in our present study and the companion study of Galeski et al.[23] indicates that activity in the amorphous material as an independent mechanism ceases by locking early in monotonic deformation, leaving the crystalline deformation processes as the dominant ones.

In our study the principal goal was to determine the resistances of the active crystallographic deformation mechanisms which can then be used in computational models to predict more complex deformation modes of semicrystalline polymers of the type discussed by Ahzi et al.[26] The mechanistic interpretations of the levels of deformation resistance of the specific slip systems and their dependence on normal stress, by the approaches of crystal plasticity, remain to be done in the future.

Acknowledgment. This research was supported by a DARPA-URI program administered by the ONR under Contract No. N00014-86-K-0768. We are grateful to A. Galeski, D. M. Parks, and S. Ahzi for many useful discussions. We also acknowledge the many contributions of H. H. Song and L. Lin in the development of the experimental techniques utilized in the present study.

Appendix

Resolved Shear Stresses for Various Deformation Mechanisms in Orthorhombic Polyethylene Crystals. The plastic deformation of single crystals (or highly textured quasi-single-crystalline material) may proceed by many possible deformation mechanisms. However, under an applied stress, with principal axes oriented in a specific way relative to the crystal axes only some of these mechanisms can be activated. Among many possible slip systems or other deformation mechanisms for a given crystal, the one on which the resolved shear stress first reaches the characteristic deformation resistance (critical resolved shear stress) will dominate in the deformation process. Thus, the knowledge of the dependence of resolved shear stress for particular deformation mechanisms on the stress state is very helpful in the analysis of the constituent plastic deformation mechanisms. Consider the single crystal under uniaxial tension (or compression), as shown in Figure 31. In the coordinate system with x_1 parallel to the tensile axis, the applied stress tensor is

$$\sigma_{ij} = \begin{vmatrix} \sigma & 0 & 0 \\ 0 & 0 & 0 \\ 0 & 0 & 0 \end{vmatrix} \tag{A1}$$

The resolved shear stress on a given slip system can then be determined by transforming σ_{ij} to a coordinate system in which x_1' corresponds to the slip direction and x_2' to the slip plane normal. In these coordinates the resolved shear stress is[28]

$$\tau = \sigma_{12}' = \sigma \cdot \cos \zeta \cos \phi = m \cdot \sigma \tag{A2}$$

where ζ is the angle between the tensile axis x_1 and the slip direction x_1' and ϕ is the angle between x_1 and the slip plane normal x_2'. The coefficient m is often called the Schmid factor. Equation A2 allows the direct calculation of the resolved shear stresses for a given orientation of tensile or compression axes. However, it is frequently more useful to plot the resolved shear stress as a function of orientation of the external stress in the stereographic projection of the crystal under consideration. To do this for an orthorhombic crystal, such as polyethylene, it is helpful to rewrite eq A2 in the form

$$\tau = \sigma \cdot m = \sigma \cdot \cos (\psi - \alpha) \cos (\psi - \beta) \sin \theta \cos (\theta - \gamma) \tag{A3}$$

where angles ψ and θ describe the orientation of the loading direction, y (see inset of Figure 12 for definition) with respect to the crystallographic unit cell (ψ is the angle between the [100] direction in the crystal and the projection of y on the (001) plane, and θ is the angle between the [001] direction and y). Moreover, α, β, and γ describe the orientation of the plane and direction of the shear of the particular deformation mechanism considered, where α is the angle between the [100] direction and the projection of the shear plane normal onto the (001) plane, β is the angle between the [100] direction and the projection of the direction of the shear onto the (001) plane, and γ is the angle between the [001] direction and the shear direction. Using eq A3 the dependences of the Schmid factor, m, on the orientation of the loading direction for possible deformation mechanisms in orthorhombic polyethylene were calculated and plotted in a stereographic projection normal to the [001] direction (chain axis direction). Parts a–h of Figure 32 present the plots obtained for the (100)[001], (010)[001], and (110)[001] chain slips, the (100)[010] and (010)[100] transverse slips, and the {110}⟨110⟩ and {310}⟨130⟩ twinning modes. These plots have been found extremely useful in both the design of the specimen geometry for the study of a particular deformation mechanism and the analysis of the deformation process observed experimentally. They allow the straightforward determination of the directions of uniaxial load for which plastic deformation should proceed according to a single mechanism, as well as those directions for which several mechanisms may compete. For example, comparison of parts a and b of Figure 32 leads to the immediate conclusion that, if the load is applied in the direction located between the [100] and [001] directions, the resolved shear stress for (010)[001] chain slip is equal to 0, whereas that for (100)[001] chain slip takes on high values, so that the latter slip system should be the predominant deformation mechanism during the deformation under that applied stress.

References and Notes

(1) Bowden, P. B.; Young, R. J. *J. Mater. Sci.* **1974**, *9*, 2034.
(2) Haudin, J. M. In *Plastic Deformation of Amorphous and Semicrystalline Materials*; Escaig, B., G'Sell, C., Eds.; Les Editions de Physique: Paris, 1982; p 291.
(3) Ward, I. M. *Mechanical Properties of Solid Polymers*, 2nd ed.; Wiley-Interscience: New York, 1983.
(4) Lin, L.; Argon, A. S., to be published.
(5) Keller, A.; Rider, J. G. *J. Mater. Sci.* **1966**, *1*, 389.
(6) Hinton, T.; Rider, G. J. *J. Appl. Phys.* **1968**, *39*, 4932.
(7) Young, R. J.; Bowden, P. B.; Ritchie, J. M.; Rider, J. G. *J. Mater. Sci.* **1973**, *8*, 23.
(8) Shinozaki, D. M.; Groves, G. W. *J. Mater. Sci.* **1973**, *8*, 1012.
(9) Pope, D. H.; Keller, A. *J. Polym. Sci., Polym. Phys. Ed.* **1975**, *13*, 533.
(10) Burnay, S. G.; Groves, G. W. *J. Mater. Sci.* **1978**, *13*, 639.
(11) Peterson, J. M. *J. Appl. Phys.* **1968**, *39*, 4920.
(12) Hinton, T.; Rider, G. J.; Simpson, A. *J. Mater. Sci.* **1974**, *9*, 1331.
(13) Young, R. J.; Bowden, P. B. *Philos. Magn.* **1974**, *29*, 1061.
(14) Frank, F. C.; Keller, A.; O'Connor, A. *Philos. Mag.* **1958**, *3*, 64.
(15) Allan, P.; Crellin, E. B.; Bevis, M. *Philos. Mag.* **1973**, *27*, 127.
(16) Lewis, D.; Wheeler, E. J.; Maddams, W. F.; Preedy, J. E. *J. Polym. Sci., Polym. Phys. Ed.* **1972**, *10*, 369.
(17) Burnay, S. G.; Groves, G. W. *Br. Polym. J.* **1978**, *10*, 30.
(18) Bowden, P. B.; Young, R. J. *Nature Phys. Sci.* **1971**, *269*, 23.
(19) Gray, R. W.; Young, R. J. *J. Mater. Sci., (Lett.)* **1974**, *9*, 521.
(20) Song, H. H.; Argon, A. S.; Cohen, R. E. *Macromolecules* **1990**, *23*, 870.
(21) G'Sell, C.; Boni, C.; Shrivastava, S. *J. Mater. Sci.* **1983**, *18*, 903.
(22) Wunderlich, B.; Cormier, C. M. *J. Polym. Sci., Polym. Phys. Ed.* **1967**, 987.
(23) Galeski, A.; Bartczak, Z.; Argon, A. S.; Cohen, R. E. *Macromolecules*, in press.
(24) Bank, M. I.; Krimm, S. *J. Polym. Sci., Polym. Phys. Ed.* **1969**, *7*, 1785.
(25) Young, R. J.; Bowden, P. B. *J. Mater. Sci.* **1973**, *8*, 1177.
(26) Ahzi, S.; Argon, A. S.; Bartczak, Z.; Parks, D. M.; Lee, B. J., to be published.
(27) Popli, R.; Mandelkern, L. *J. Polym. Sci., Polym. Phys. Ed.* **1987**, *25*, 441.
(28) Schmid, E.; Boas, W. *Plasticity of Crystals*; Hughes: London, 1950.
(29) Lin, L.; Argon, A. S., to be published.

Registry No. HDPE, 9002-88-4.